2015

Shallow Water Depth Inversion Based on Data Mining Models

Shu Gao
Louisiana State University and Agricultural and Mechanical College, sgao7@lsu.edu

SHALLOW WATER DEPTH INVERSION BASED ON DATA MINING MODELS

A Thesis

Submitted to the Graduate Faculty of the
Louisiana State University and
Agricultural and Mechanical College
in partial fulfillment of the
requirements for the degree of
Master of Science

in

The Department of Geography and Anthropology

by
Shu Gao
B.S., China University of Petroleum (East China), 2013
December 2015

ACKNOWLEDGEMENTS

Firstly, I would like to thank my supervisor Dr. Lei Wang for his guidance and support throughout my master studies. His instruction and experience gave me much confidence when I started working on my research. It is my honor to complete my master study under his supervision.

Besides, I would also like to thank Dr. Zhiqiang Deng and Dr. Xuelian Meng for the time and support they have given to me while serving as committee members. Especially, I am appreciate that Dr. Deng for offering me a student worker position, which is helpful for my research.

My sincere thanks also go to my advisor Dr. Lei Wang, Dr. Fahui Wang and Dr. Jianhua Wan from China University of Petroleum. I very appreciate their patient writings on the recommendations for my Ph.D. application.

Last but not the least, I would like to thank my parents, Hua Su and Guangzhong Gao for supporting me spiritually throughout writing this thesis and my life in general. Without their coontinues support, I would not be where I am today.

TABLE OF CONTENTS

LIST OF TABLES

LIST OF FIGURES

NOMENCLATURE

ANN - Artificial Neural Networks

BP-ANN - Back- Propagation Artificial Neural Network

CART - Classification and Regression Tree

CP - Complexity Parameter

GIS - Geographic Information System

JALBTCX - Joint Airborne LiDAR Bathymetry Technical Center of Expertise

LIDAR - Light Detection and Ranging

MSE - Mean Squared Errors

NAD83 - North American Datum of 1983

r - Correlation Coefficient

RMSE - Root Mean Square Error

SAR - Synthetic Aperture Radar

SSR - Sum of Squared Residuals

SVM – Support Vector Machine

USACE - U.S. Army Corps of Engineers

ABSTRACT

This thesis focuses on applying machine-learning algorithms on water depth inversion from remote sensing images, with a case study in Michigan lake area. The goal is to assess the use of the public available Landsat images on shallow water depth inversion. Firstly, ICESat elevation data were used to determine the absolute water surface elevation. Airborne bathymetry Lidar data provide systematic measure of water bottom elevation. Subtracting water bottom elevation from water surface elevation will result in water depth. Water depth is associated with reflectance recorded as DN value in Landsat images. Water depth inversion was tested on ANN models, SVM models with four different kernel functions and regression tree model that exploit the correlation between water depth and image band ratios. The result showed that the RMSE (root-mean-square error) of all models are smaller than 1.5 meters and the R^2 of them are greater than 0.81. The conclusion is Landsat images can be used to measure water depth in shallow area of the lakes. Potentially, water volume change of the Great Lakes can be monitored by using the procedure explored in this research.

CHAPTER 1. INTRODUCTION

Bathymetric data is widely used for ship navigation, underwater construction, water resources management, flood disaster monitoring, aquaculture, and military operations. Traditionally, bathymetry survey was performed by using echo-sounding apparatus and multi-beam bathymetric system mounted on vessels, with high cost and low efficiency (Zhang, 2013). From 1960s, remote sensing technology has found a new way for bathymetric mapping and morphological characterization of seabed. Overall, nowadays, there are several remote sensing techniques that can be used as a source to derive bathymetry data along coastal areas including sonar (sound navigating), LIDAR (light detection and ranging) and high-resolution satellite images (Vojinovic, 2013). Compared with traditional methods, remote sensing is superior at its low cost, wide coverage, and high repetitive frequency. Shallow water depth inversion from multispectral remote sensing images could provide reliable measure of water depth and bottom bathymetry (Zhang, 2009). Empirical models have been proposed for bathymetric data estimation. Among them, Artificial Neural Network (ANN) and Support Vector Machine (SVM) have proved to be effective in modeling virtually any nonlinear function with acceptable accuracy (Suryanarayana, 2013). Bierwirth (1984) and Lafon (2001) combined theoretical models and experimental parameters based on Landsat TM and SPOT image respectively. Su et al. (2008) and Raj et al. (2013) used IKONOS and Landsat TM image with non-linear inversion model to estimate water depth. Sandidge and Holyer, Wang (1998) utilized a back-propagation artificial neural network (BP-ANN) method to develop the relationship between reflectance and observed water depth.

In this thesis, multiple machine learning methods, such as ANN, SVM and regression tree were applied to build water depth inversion models on a selected Landsat image and the results are compared and discussed.

1.1 REGIONAL BACKGROUND

The Great Lakes are located in northeastern North America. They are Lake Erie, Lake Huron, Lake Michigan, Lake Ontario and Lake Superior, a series of interconnected freshwater lakes on the Canada-United States border. The Great Lakes contains about 23,000 km^3 of water. The volume of water is enough to flood the continental United States to a depth of nearly 3 m. Moreover, it covers a total area of 244,000 km^2 with 16,000 km of coastline. Lake Michigan is the largest lake and is the only one entirely within one country.

In 2013, the year brought a new record low water level for Lake Michigan, which is 175.57 meters above sea level. The former record was 175.63 meters above sea level in 1964 (Hayden, 2013). The low water levels will force shippers to lighten their loads and increase costs so that vessels can get into ports (Hayden, 2013). For solving the problem, government has spent money to open up more areas of the lake to boaters.

1.2 WATER-DEPTH REMOTE SENSING PRINCIPLE

The fundamental physical principle of water depth inversion models is that electromagnetic energy leaving water body from the water bottom is attenuated by water volume. The deeper the water, the more attenuation. The brightness tune of shallow water area recorded in the images is largely determined by the depth of water. Deep areas have low digital number (DN) values in the image since the water absorbs much of the reflected light. Shallow areas have high DN values since less light reflected from the seabed (Raj, 2013).

As showed in Figure 1.1, water absorbs most electromagnetic energy leaving the bottom. The lights with wavelength over 0.75 micrometer are completely absorbed. Water are completely dark in near infrared wavelengths and beyond. Therefore, for water depth estimation, only visible bands, especially the green band and blue band are used to build the inversion models. In this research, I used band 1 (blue) and 2 (green) of Landsat data.

Other than water depth, turbidity is another factor that could affect the brightness of water. Turbid water has higher reflectance than clear water. This is also true for waters containing high chlorophyll concentrations. These reflectance patterns are used to detect algae colonies as well as contaminations such as oil spills or industrial wastewater (Campbell, 2007). However, the influence of these environmental factors is still relatively small. In this research, they are not considered in the models.

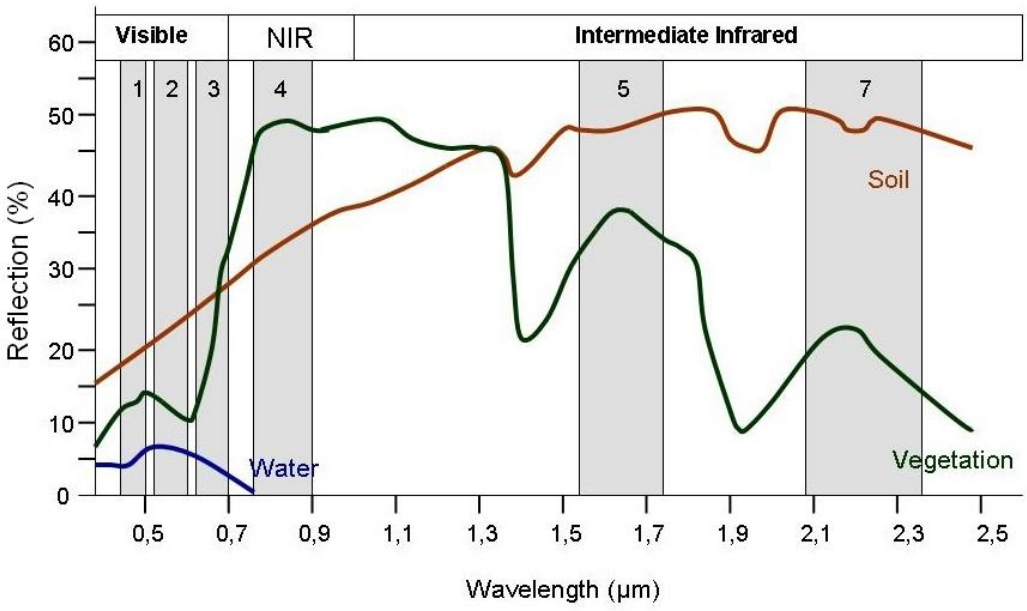

Figure 1.1 Spectral Signatures of Soil, Vegetation and Water, and Spectral Bands of LANDSAT7
(Source: Siegmund, Menz 2005**)**

1.3 OBJECTIVES AND PROCEDURE

This research aims to apply data mining methods on satellite images in building shallow water depth inversion models to evaluate the performance and feasibility of the models. This is accomplished through seven tasks outlined below.

1. Utilize ICESat data and Bathymetry LiDAR data to calculate the water depth.
2. Use regression tree model as the water depth inversion model.
3. Use ANN models as the water depth inversion model.
4. Use different Kernel Functions of Supporting Vector Machine (SVM) method as water depth inversion model. The different Kernel Functions of SVM method are compared to find the best model.
5. Compare the shallow water depth inversion models of ANN, SVM and regression tree.
6. Apply the water depth inversion models to measure water depth.

CHAPTER 2. LITERATURE REVIEW

2.1 DATA

The Ice, Cloud and Land Elevation Satellite (ICESat) was launched by the National Aeronautics and Space Administration (NASA) on January 13, 2003 and ended on August 14, 2010. The on-board Geoscience Laser Altimetry System (GLAS) collects laser reflection from ground and clouds. The ground returns measure surface elevation at great accuracy (15cm) covering most lands and water bodies of the earth. The application of the ICESat data have been used in far more aspects than the initial purpose. The major applications of GLAS data include measurement of sea-ice freeboard, land elevation and forest height, change detection of Antarctic and Greenland ice sheets elevation, Land cover classification, Urban building height extraction and water level changes in lakes (Wang et al., 2011). An overview of the ICESat Mission including its objections, requirements, mission description, data products are documented in Schutz et al. (2005). Zwally et al. (2002) stated the ICESat's laser measurements of many aspects in considerable detail including the GLAS instrument characteristics, data products, applications of data and so on. Both articles agreed that GLAS data could be effective alternative to monitoring of water levels of selected rivers and lakes. Chipman and Lillesand (2007) used MODIS and ICESat data to assess the dynamics of new lakes in southern Egypt. The results showed that two of the new lakes have already disappeared and several remaining lake will disappear shortly. So the articles can prove that ICESat data can be used well in different applications.

Along with the satellites, airborne scanning LiDAR also provides reliable and accurate 3D measurement of surface elevation, from which high-resolution Digital Terrain Models (DTMs) can be derived for geomorphological studies (Hohenthal, 2011; Hofel, 2011). Laser scanning is

now a widespread means of obtaining precise and high-resolution three-dimensional (3D) topographic information, with high efficiency and ease of use (Belian, 2005; Buckley, 2008; Hodgetts, 2009). Bathymetric LiDAR utilizes a green laser to penetrate through water to the bottom for the bathymetry of coastal areas. The U.S. Army Corps of Engineers (USACE) Joint Airborne LiDAR Bathymetry Technical Center of Expertise (JALBTCX) collected the bathymetry LiDAR data and published the data for public use. JALBTCX collected its first airborne coastal mapping data on the Great Lakes in 1995 (Reif, 2013). Since then, the JALBTCX has collected nearly 5 billion elevation and depth measurements and created over 2000 geographic information system (GIS) products for the shorelines of the Great Lakes (Reif, 2013). The applications of bathymetry LiDAR include shoreline and elevation change analysis, submerged sediment characterization, bluff edge detection, invasive species identification and so on. Coastal researchers, engineers, and managers can utilize these applications to increase understanding of coastal processes, evaluate engineering solutions and examine their performance, and inform coastal planning and decision-making (Reif, 2013).

Accurate bathymetric measurements are of fundamental importance for monitoring sea bottom. Retrieving bathymetric information from satellite imagery data is regarded as a fast and economically advantageous solution to automatic water depth calculation in shallow water (Stumpf et al., 2003 and Su et al., 2008). The primal attempts for automatic estimation of shallow water depth were based on the combination of multispectral data and radiometric techniques (Lyzenga, 1978). In the following years, with the advance of remote sensing technology, high resolution images have become available, such as Ikonos, Quickbird and Worldview-2 data (Doxani, 2012). However, the high cost of the high resolution images and small spatial temporal coverage prevent these images to be widely adopted by the research community. Instead, Landsat

images have consistent long time coverage and are made free to the public by the USGS. It is interesting to provide evaluation of feasibility of Landsat images on shallow water depth inversion in concern of the low resolution problem (Conger et al., 2006; Su et al., 2008).

2.2 SHALLOW WATER INVERSION METHODS

A wide variety of empirical models have been proposed and tested for bathymetric estimations by using the statistical relationship between satellite image pixel values and field measured water depth (Doxani, 2012). One of the most widely used method is the inversion method proposed by Lyzenga (1978, 1981, 1985). The model assumes the bottom reflectance and water depth can be described by an exponential function. The parameters of the exponential function are estimated through least-squared fitting on field sample data. Stumpf et al. (2003) presented an algorithm using a ratio of reflectance in replace of reflectance data. The result showed that by doing so, there was significant improvement over the standard inversion models. In addition, the model could estimate water depth even over 25 m. Recently, there have been a blooming of research activities to develop water depth models from satellite images. The water depth inversion model proposed by Zhang (2013) uses a single band and band ratios to derive bathymetry from a Linear model, a Logarithmic model, a Power exponential model and an Exponential model. The paper showed that the power exponential model based on Landsat band 2 is the best among other alternatives. The log-linear inversion model by Raj et al. (2013) used data from multiple bands images and bathymetry measure from echo sounder. The RMSE of the method in the paper was 1.9513 meters. The non-linear bathymetric inversion model by Stumpf et al. (2003) used log-transformed band ratio to eliminate errors due to different attenuation coefficients from multiple bands. Another non-linear inversion model derived by Su et al. (2008) was based on a localized regression algorithm on IKONOS high resolution image and bathymetry data. They

found that the localized model was able to compensate the variability of bottom conditions. Doxani et al. (2012) derived shallow water bathymetry using Lyzenga linear bathymetry model to extract the water depth information from Wordview-2 data and echo sounding. Liu et al. (2010) carried out a work on bathymetric depth inversion using a single-band model and a dual-band model based on SPOT-5 data. The result showed that the dual-band model was better than the single band model. The RMSE of the dual-band model was 1.87 meters. Fan et al. (2008) used wave-number spectrum technique to retrieve coastal water depths by the Synthetic Aperture Radar (SAR).

In addition to above methods, many authors use the data mining methods to retrieve water depth. Thomas (2012) used regression tree model to map groundwater depth in the Zinder region. Yasa (2013) applied classification and regression trees method for predicting the scour depth. Huang et al. (2010) utilized the stepwise regression tree to estimate the subpixel land cover. Artificial Neural Networks (ANN) provides a fast and practical solution for depth estimation in shallow waters (Raj, 2013). Zhang (2011) used IKONOS satellite image to inverse water depth based on bands ratio and an ANN method. Huang et al. (2009) employed a back-propagation artificial neural network (BP-ANN) method to derive water depth (Huang, 2009). The image they used was from Landsat 7. The reported RMSE was about 0.7 meters. Wang (2007) applied a momentum BP neural network (MBPNN) for water depth based on Landsat 7 images. Sandidge (1998) measured the depth of the Florida Keys and Tampa Bay using ANN method based on AVIRIS data and echo sounding data. The RMS of their experiments were 0.39 meters and 0.84 meters respectively. To the knowledge of the author, there has not been any research efforts to evaluate the use of Support Vector Machine (SVM) method on water depth inversion, although it has been used in many aspects of remote sensing applications, such as a water quality mapping application in Smola (1998).

From the literature review, it is clear that machine-learning methods have been adopted in many recent research works for water depth estimation from satellite images. However, it was not clear which of the methods should be adopted to map the Great Lakes coastal area, as there was no any prior research works mentioned in the literature. In addition, the SVM method was among the machine-learning methodology, but was not well documented or tested. This research will focus on comparing the machine-learning algorithms on water depth retrieval, especially on including the SVM method in the experiments.

CHAPTER 3. STUDY AREA AND DATA PROCESSING

3.1 STUDY AREA

As showed in Figure 3.1, the study site is located in the west shallow areas of Lake Michigan and lies between latitudes 41° 45′ 25.764″ N and 41° 57′ 29.239″ N, and between longitude 86° 34′ 23.164″ W and 86° 50′ 9.439″ W. It was close to Michigan City. It assumed that the water quality were homogeneous and the bottom was uniform in the study area.

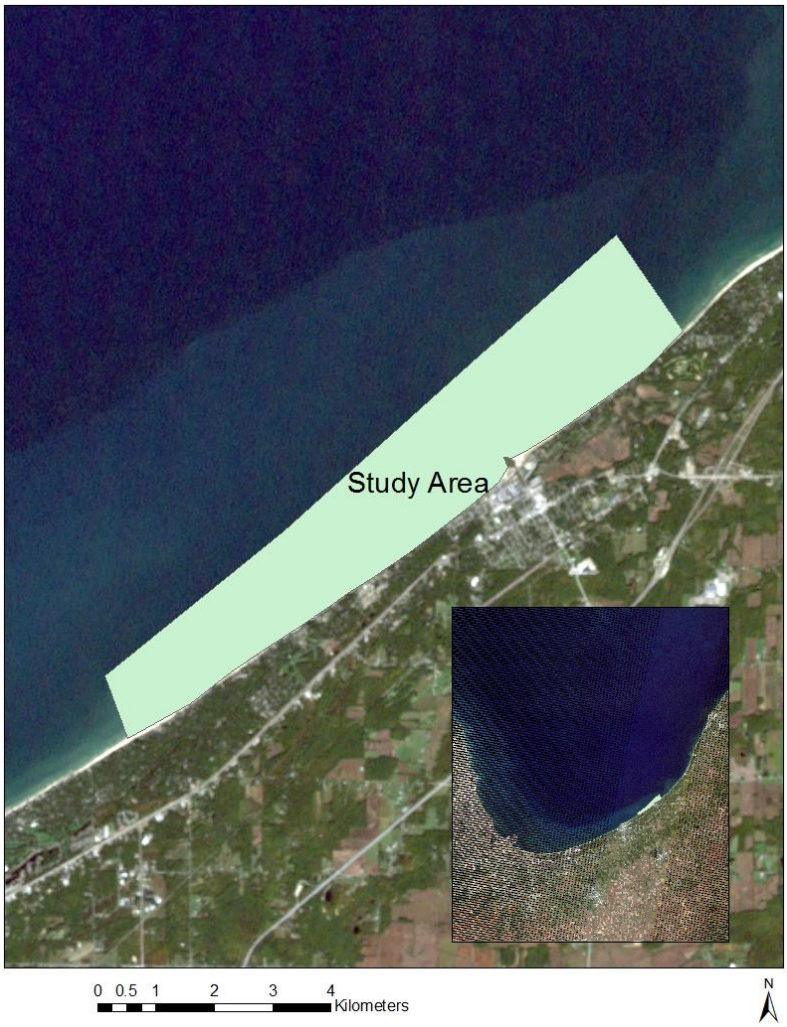

Figure 3.1 Study Area

3.2 DATA ANALYSIS

3.2.1 ICESat Data

This research used the ICESat data product GLA06, which provides global elevation data. This product includes elevation data for both land and water bodies, covering most part of the earth. The ICESat data points (Figure 3.2) were obtained on December 23, 2008 during one of the ICESat campaigns. The surface water elevation at these points are listed in the Table 3.1. These twelve points are ordered from the coastline towards the lake. The water surface elevation readings at these points are very consistent. The average water surface elevation is 175.42 meters. This value is used as the surface elevation, from which the water bottom elevation is subtracted to obtain water depth.

Figure 3.2 ICESat Data

Table 3.1 The Elevation of Water Surface

Point	Elevation (meter)	Point	Elevation (meter)
1	175.105308	7	175.336462
2	175.356333	8	175.457487
3	175.392359	9	175.385513
4	175.527385	10	175.569538
5	175.44041	11	175.462564
6	175.414436	12	175.44059

3.2.2 Landsat 7 Data

The pixel values for water depth inversion is obtained from Landsat 7. It can be download from USGS (https://earthexplorer.usgs.gov). The Landsat 7 imagery was acquired on October 09, 2008. The Landsat ETM+ has shown a data gap of a 22% data loss per scene due to scan line corrector failure since May 31, 2003. The data gap areas were avoided when I selected the study area. The spatial resolution and wavelength of each band is shown in Table 3.2

First, 500 points in the study area randomly selected from the three area. The 500 points are displayed in the Figure. 3.3. Another 200 points in the area shown in Figure 3.4 are randomly selected from the area for testing. The 700 pixel values of band 1-5 and band 7 were gained by extracting from the Landsat 7 images.

In order to select the best set of bands and band ratios for water depth retrieval, correlations of pixel values of the six bands (band 1-5 and band 7) and their band ratios with corresponding water depths were analyzed. A correlation matrix was built in the SPSS software for the single

Table 3.2 Basic Information of Landsat 7

Band	Wavelength (μm)	Spatial Resolution (m)
1	0.45-0.515	30
2	0.525-0.605	30
3	0.63-0.690	30
4	0.75-0.90	30
5	1.55-1.75	30
6	10.40-12.50	60
7	2.09-2.35	30
8	0.52-0.90	15

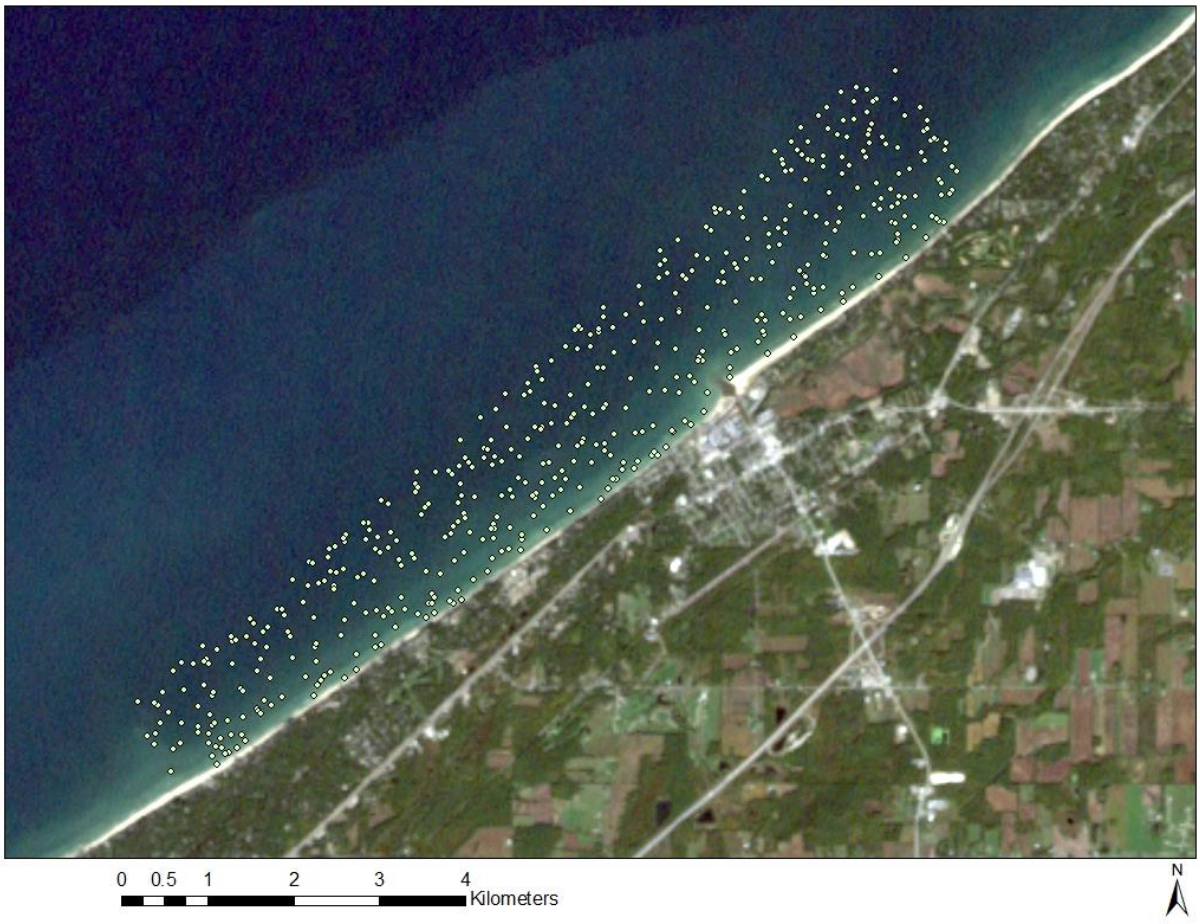

Figure 3.3 The Position of Five hundred Training Samples

Figure 3.4 The Position of Two Hundred Testing Samples

band, band ratios, band differences and band sums with water depth values from the 500 training data points. The correlation equation is

$$r = \frac{\sum_{i=1}^{N}(x_i-\bar{x})(y_i-\bar{y})}{\sqrt{\sum_{i=1}^{N}(x_i-\bar{x})^2}\sqrt{\sum_{i=1}^{N}(y_i-\bar{y})^2}} \quad (3.1)$$

where r is the correlation index, x_i is the pixel value factor, $\bar{x}$ is the average of the pixel value factor, y is water depth, $\bar{y}$ is the average of water depth, N is the number of samples.

Results showed that band2, band1/ band2, band2 – band4, band2 – band5， band2 – band7, band1 + band2 have stronger correlation with water depth than other bands and band

combinations(Table.3.3). Therefore, they were selected to retrieve water depths and adopted for further modeling. The distribution of water depth is shown in Figure 3.5. The Figure 3.6 to Figure 3.12 are the relationships between water depth and each variable.

Table 3.3 The Correlation of Six Parameters

Parameters	ETM+2	ETM+1 / ETM+2	ETM+2 - ETM+4	ETM+2 - ETM+5	ETM+2 - ETM+7	ETM+1 + ETM+2
Correlation	-0.831	0.859	-0.849	-0.833	-0.827	-0.806

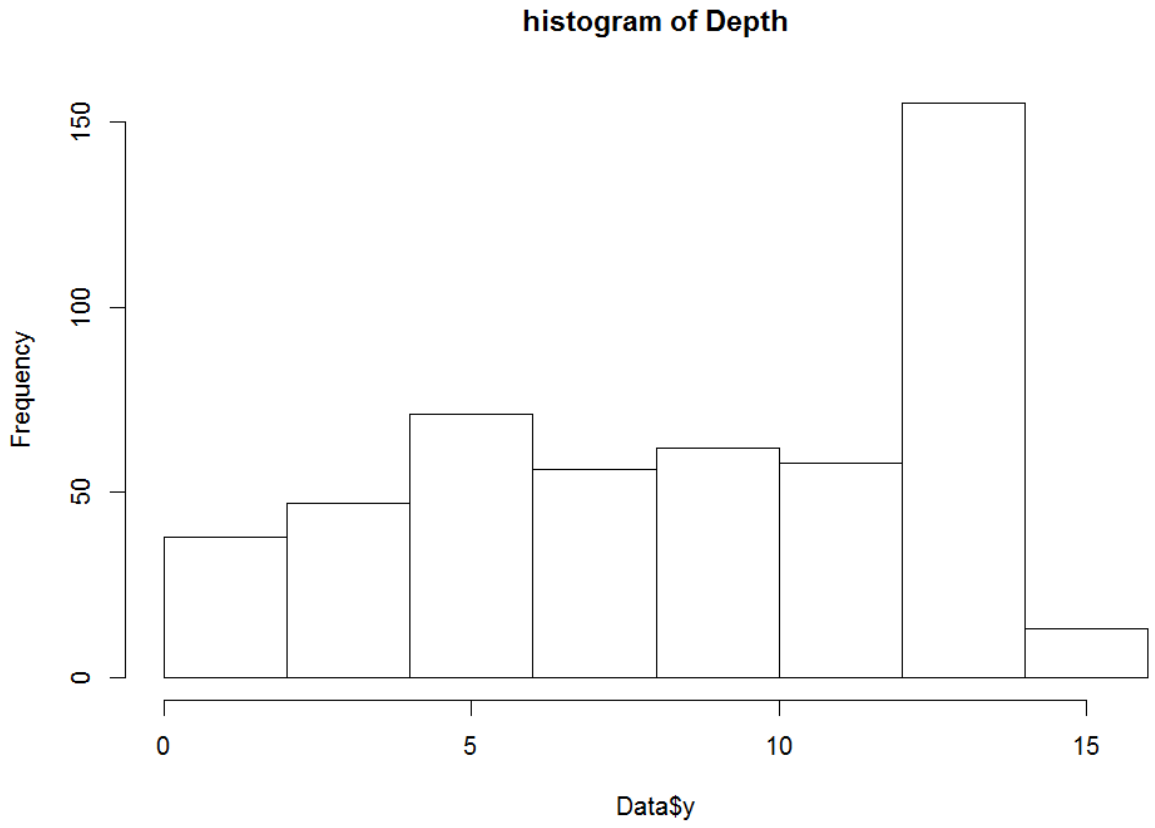

Figure 3.5 Histogram of the Depth of Training Data

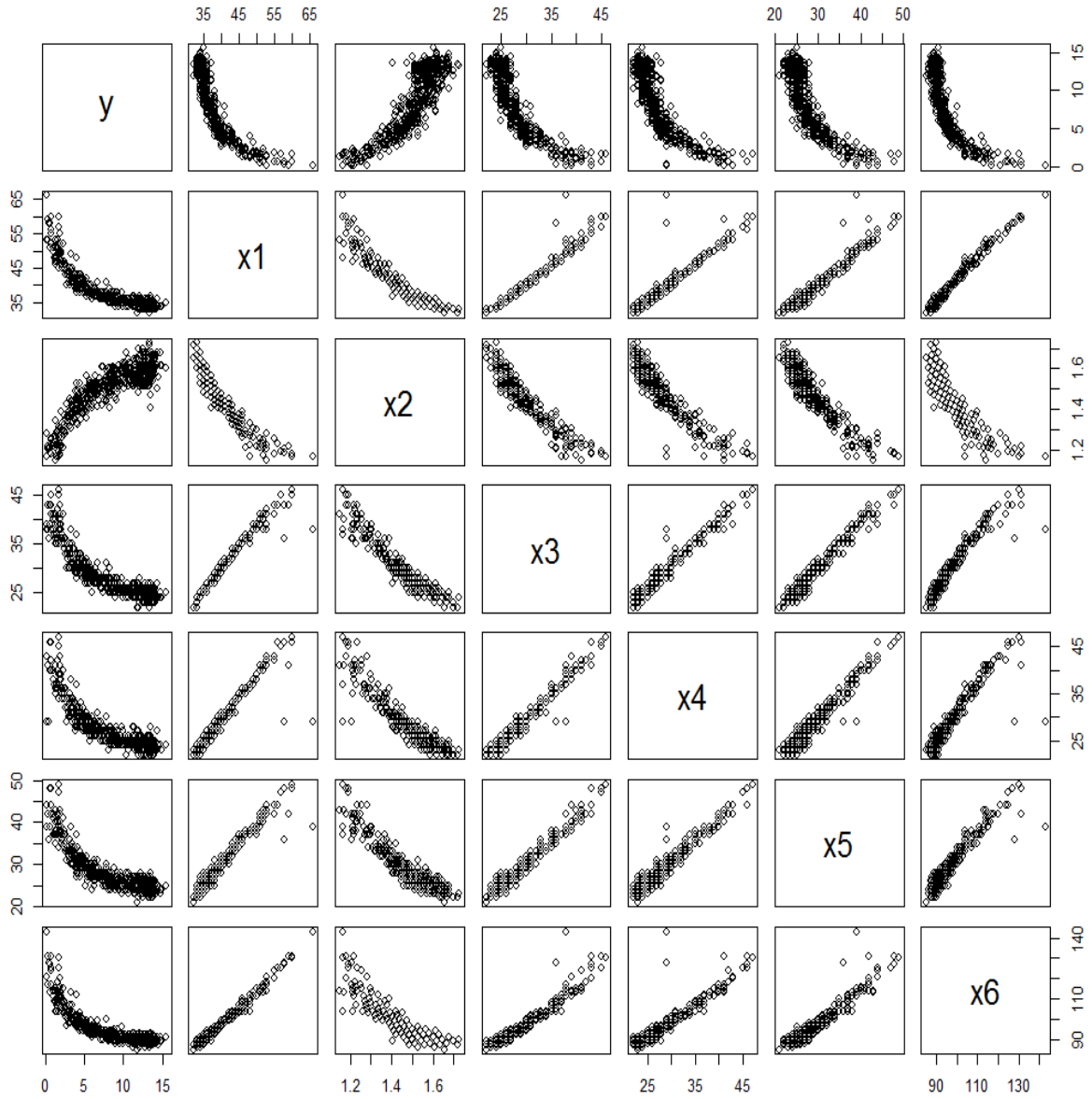

Figure 3.6 The Relationships between Each ETM+ bands

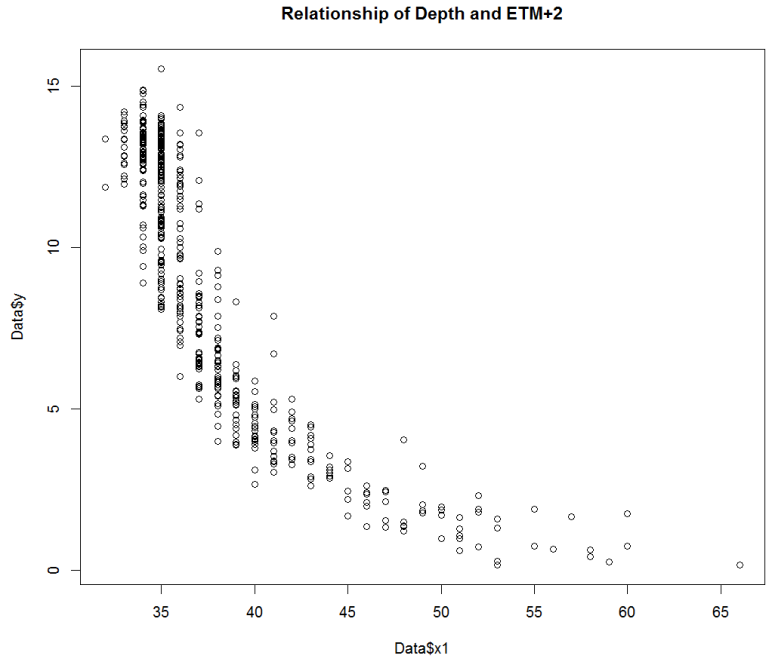

Figure 3.7 The Relationships of Water Depth and ETM+2

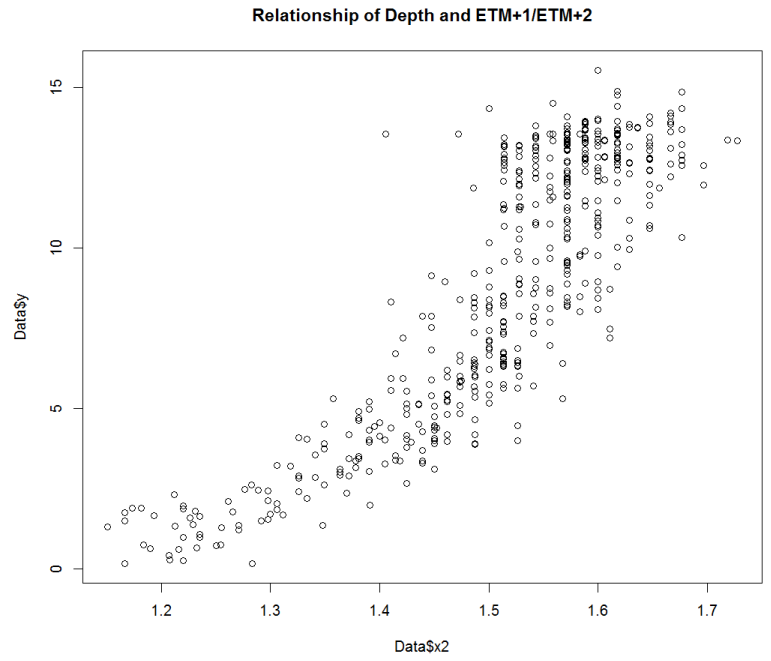

Figure 3.8 The Relationships of Water Depth and ETM+1/ETM+2

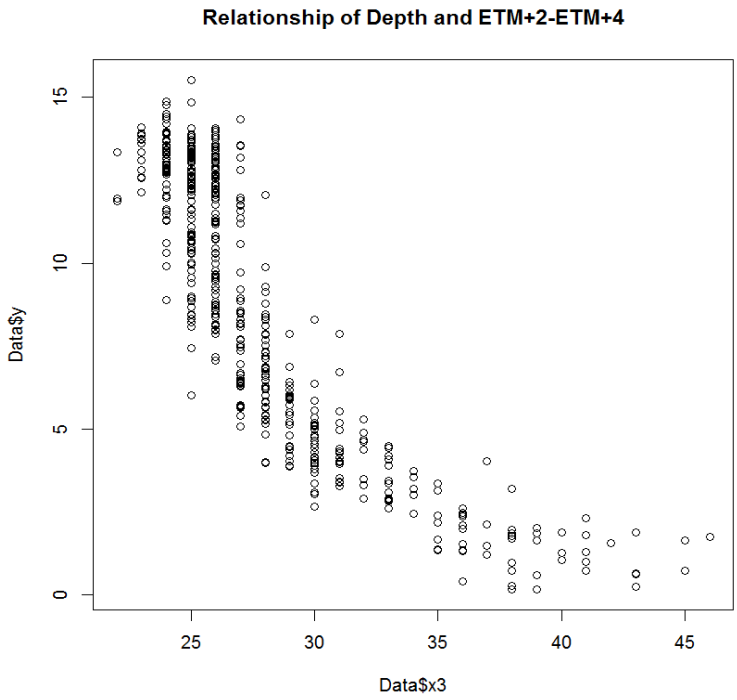

Figure 3.9 The Relationships of Water Depth and ETM+2-ETM+4

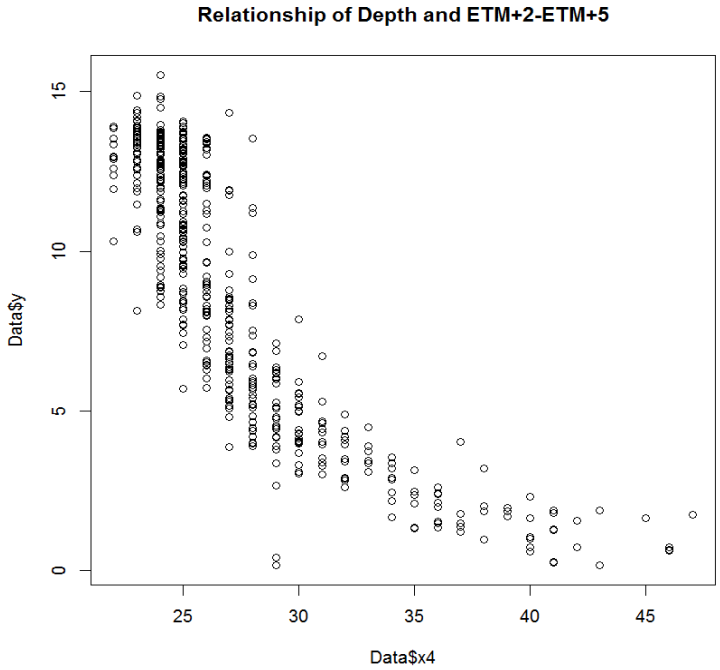

Figure 3.10 The Relationships of Water Depth and ETM+2-ETM+5

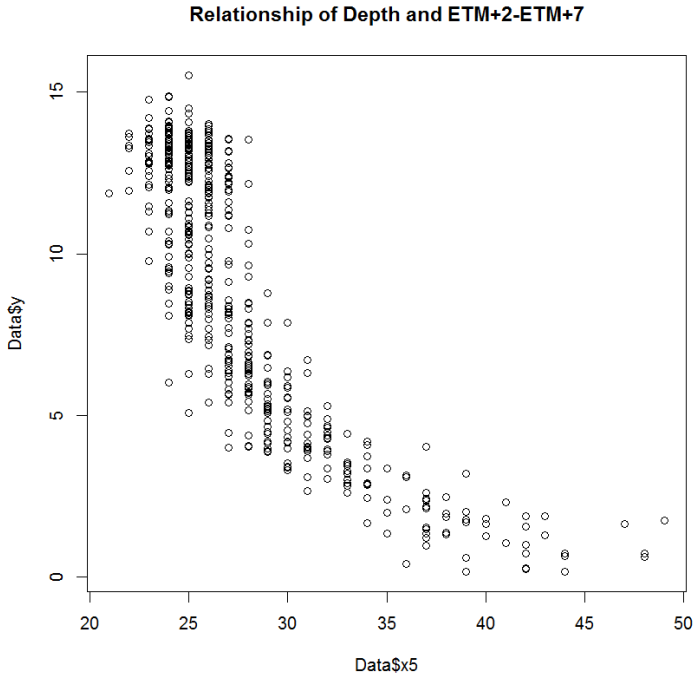

Figure 3.11 The Relationships of Water Depth and ETM+2-ETM+7

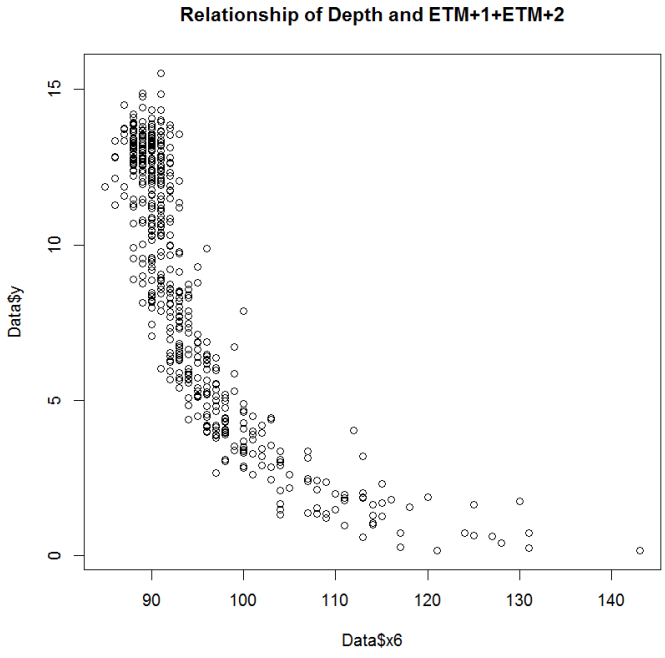

Figure 3.12 The Relationships of Water Depth and ETM+1+ETM+2

3.2.3 Bathymetric LiDAR

The U.S. Army Corps of Engineers (USACE) Joint Airborne LiDAR Bathymetry Technical Center of Expertise (JALBTCX) collected its first airborne coastal mapping data on the Great Lakes in 1995. Since then, JALBTCX has collected nearly 5 billion elevation and depth measurements and created over 2000 geographic information system (GIS) products for the shorelines of the Great Lakes. Figure 3.13 displayed the surveying region of Great Lakes. The Bathymetric LiDAR data used in this thesis part of the dataset contributed by JALBTCX through NOAA's Digital Coast Data Center. The reported vertical accuracy is 20 cm and the horizontal accuracy is 75 cm. The data are all in geographic coordinates using the North American Datum of 1983.

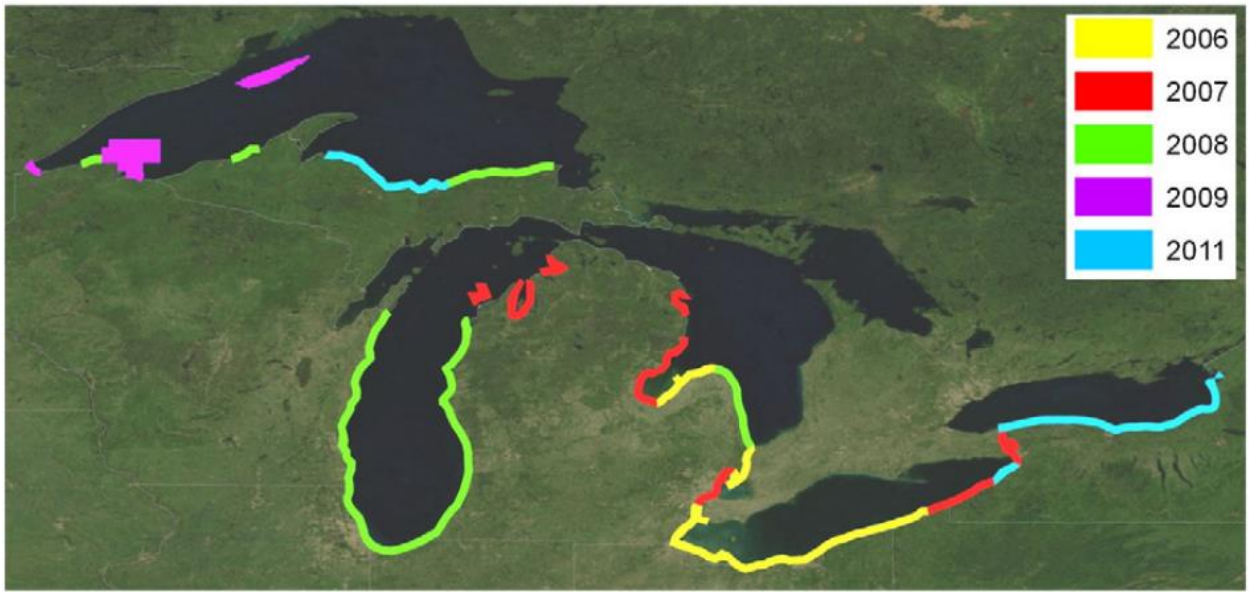

Figure 3.13 Years in which the Great Lakes Region was Surveyed under the NCMP (Reif, 2013)

For obtaining the water depth date from raw data download from the NOAA DIGITAL COAST, there are four major steps: (1) transfer format "laz" format to "las" format by using laszip software; (2) convert the LAS format from the "las" files to multipoint in ArcGIS; (3) the water is the difference of water surface elevation obtained from ICESat and the lake bottom elevation

achieved from bathymetric LiDAR. The interpolated shallow water depth in the study is shown in the following Figure (Figure 3.14). The maximal water depth in the study area is 16.2159 meters.

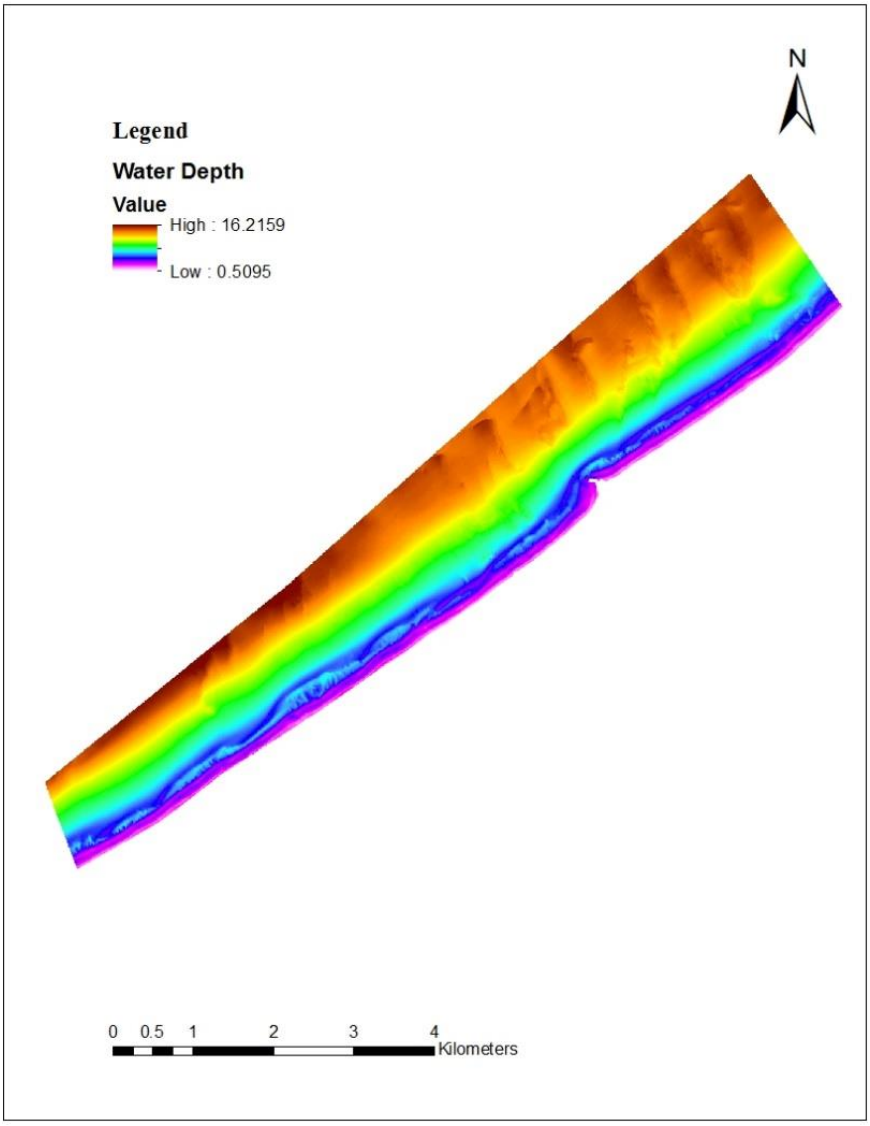

Figure 3.14 The Depth of Study Area

CHAPTER 4. REGRESSION TREE

The classification and regression tree (CART) method is a tool for numerical prediction and data classification. The regression tree algorithm is based on that of Breiman *et al*. (1984) Each deals with the prediction of a response variable y given the values of a vector of predictor variables x. CART can deal with either categorical or continuous dependent variables. With categorical dependent variables, CART produces a classification tree. If the dependent variable is continues, it will be a regression problem. In mathematical terms, the problem is to find a function $f(x)$ that maps each point in X to a point in Y. The construction of $f(x)$ requires the existence of a training sample of n observations L = $\{(x_1, y_1), \dots , (x_n, y_n)\}$. The criterion for choosing $f(x)$is usually mean squared error (MSE) for regression and expected misclassification cost for classification.

A regression tree is similarly a tree-structured solution in which a constant or a relatively simple regression model is fitted to the data in each partition (Loh, 2008). In the tree design, it is represented by branches from the same node that have different splitting predictors. At each node of the tree, the algorithm checks the value of one input x_i and depending on the (binary) answer, it will continue to the left or to the right subbranch. When the algorithm reach a leaf, it finds the prediction.

4.1 MODEL BUILDING

The open source statistic software R is used for the regression tree method. In R, CART can be generated through the "rpart" package. Using the "rpart" of R to build the regression tree, there are three major tasks: (1) how to split the data at each step, (2) when to stop splitting, (3) how to predict the depth value of the six variables. There are many approaches to the first task.

For ease of interpretation, a large majority of algorithms employ univariate splits of the form $x_i \leqslant$ c (if x_i is non-categorical). The variable x_i and the split point c are often found by an exhaustive search that optimizes a node impurity criterion such as the sum of squared residuals (SSR), mean squared errors (MSE). There are also several ways to deal with the second task, such as stopping rules and tree pruning. The aim to pruning trees is to decrease the chance of over-fitting. Once the tree is built, it is easy to make predictions: trace the tree until it reaches a leaf node.

To use "rpart" in R, there are three parameters to determine when the creating should stop. They are "cp" (complexity parameter), "minsplit", and "maxdepth". "minsplit" is the minimum number of observations that must exist in a node for a split to be attempted. "maxdepth" is the maximum depth of any node of the final tree. The default of these parameters is 0.01, 20 and 30. For avoiding over-fitting, the effectiveness of these defaults needs checking. Typically, selecting a tree size that minimizes the cross-validation error was preferred. Then, examine the cross-validated error results, select the complexity parameter associated with minimum error (xerror in R), and place it into the prune function. The correct amount of pruning is, however, usually difficult to determine. Besides, a large tree is undesirable because it is more difficult to interpret.

First of all, the "cp" was set as 0.001 for building regression tree. According to the relationship of cp and x relative error, it was found that the best size of tree was 8 when cp was 0.0023. Then, the cp was set 0.0023 for pruning tree. The Relationship between Relative Error and CP is shown in Figure 4.1. The regression tree after pruning is shown in Figure 4.2. The Figure 4.3 showed the relationship between number of Splits with the relative error and R^2.

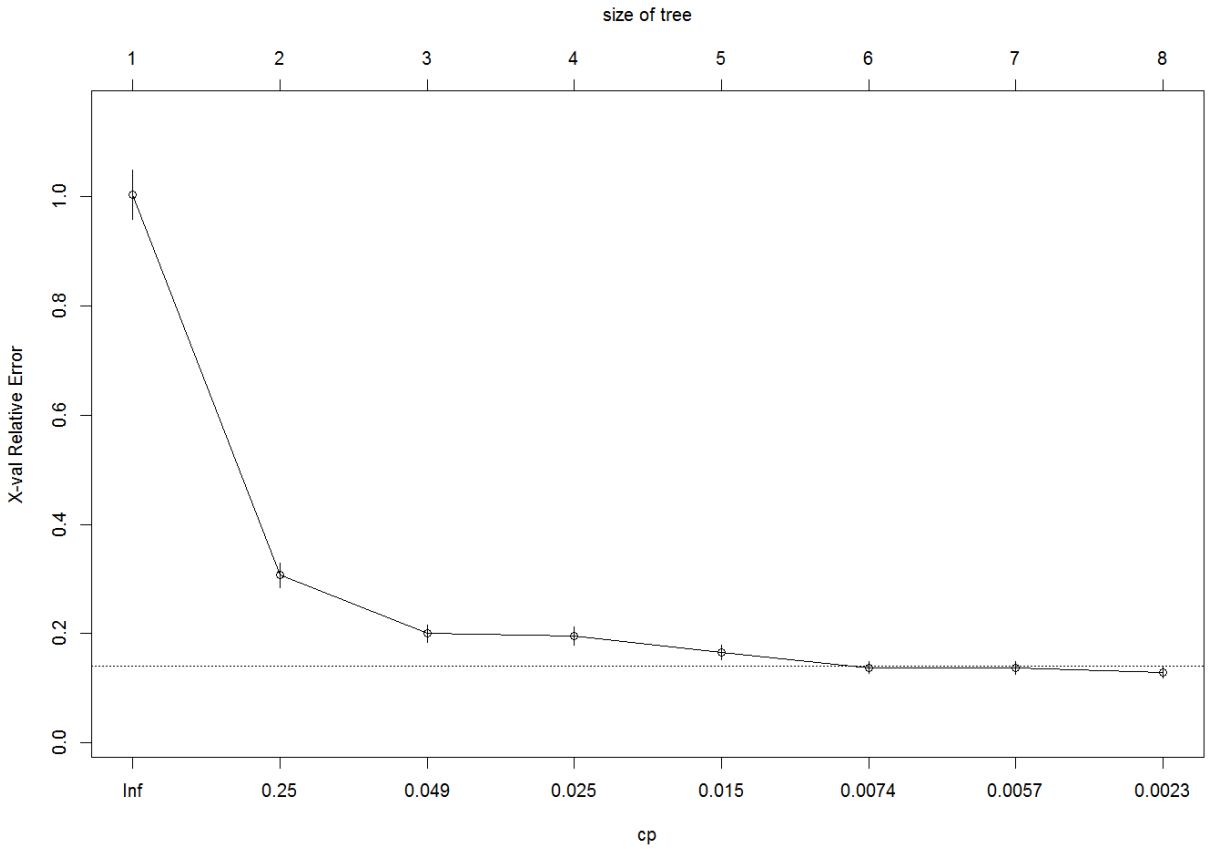

Figure 4.1 The Relationship between Relative Error and CP

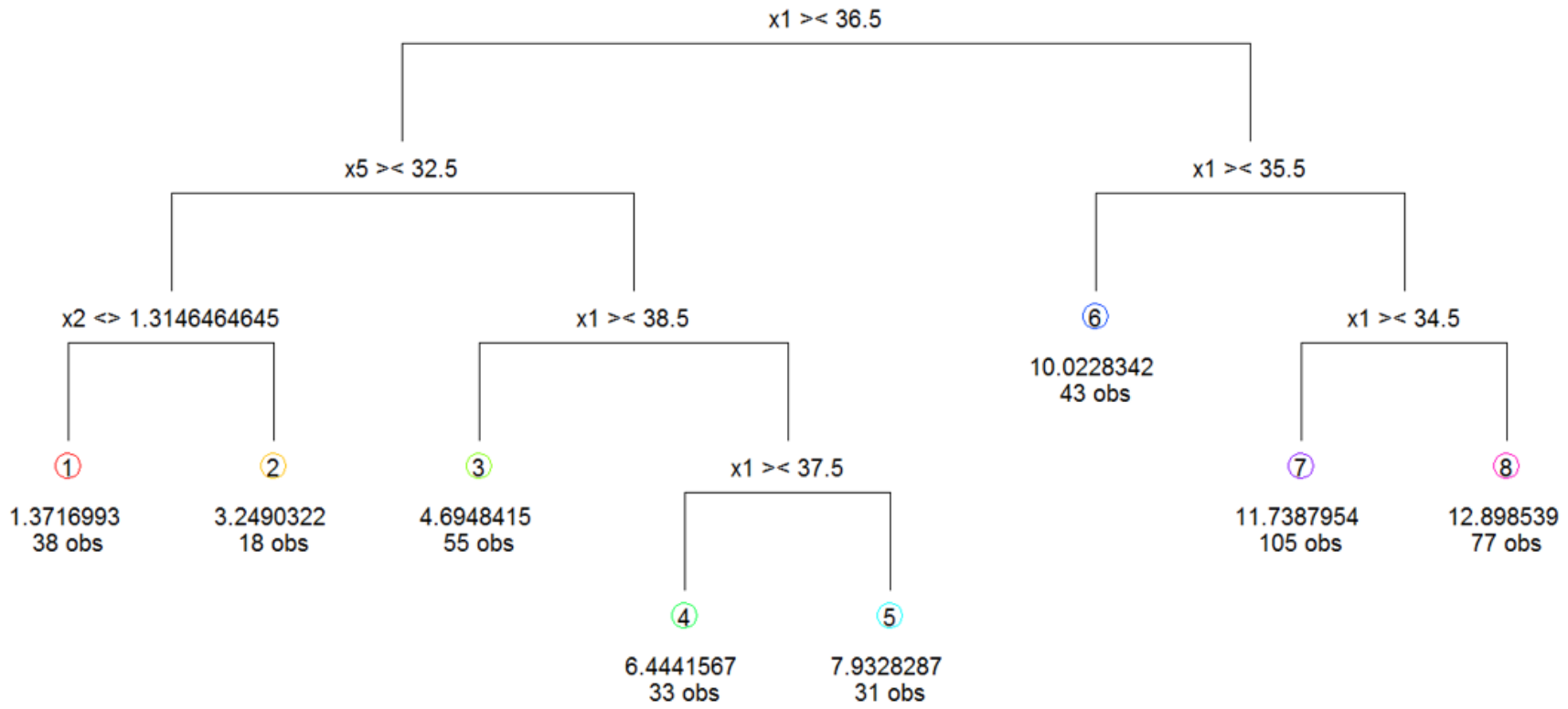

Figure 4.2 The Regression Tree after Pruning

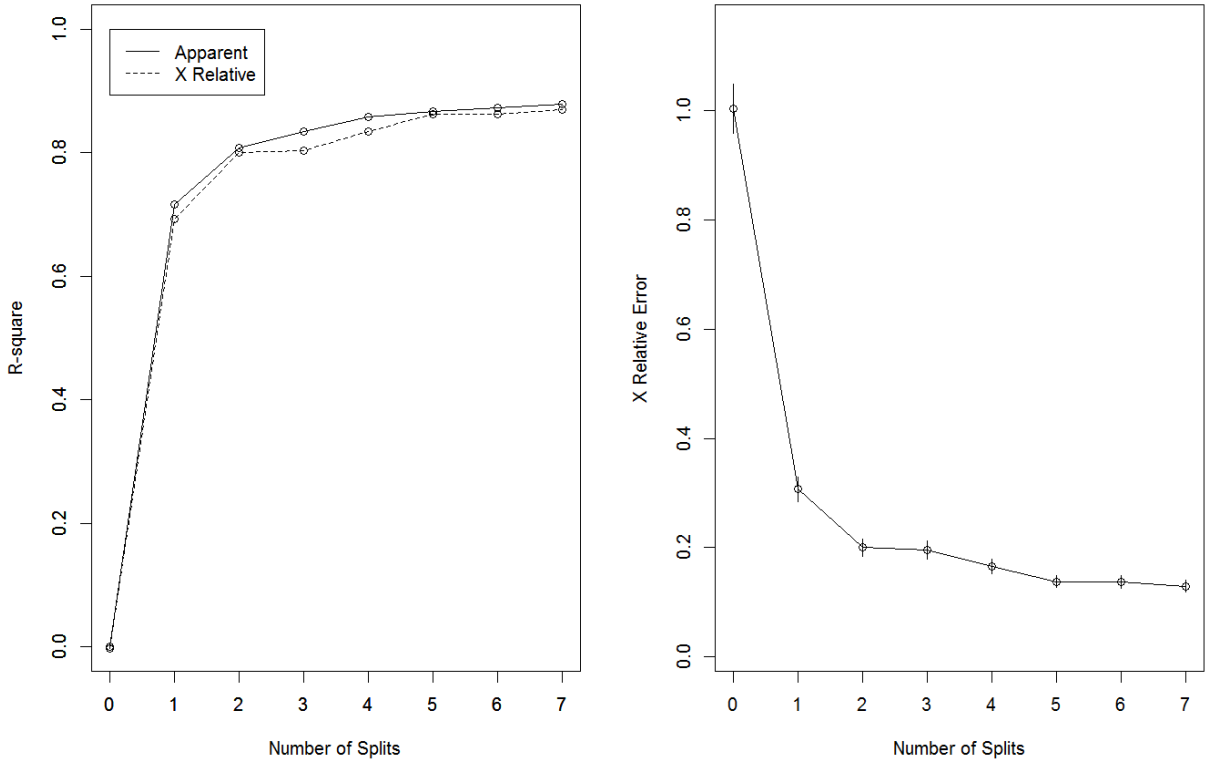

Figure 4.3 The Relationship between R^2 and Number of Splits and the Relationship between Relative Error and Number of Splits

4.2 RESULTS

For quantitative evaluation of different equations, statistical indicators such as the correlation coefficient (r), and Root Mean Square Error (RMSE) are used as follows:

$$r = \frac{\sum_{i=1}^{N}(x_i-\bar{x})(y_i-\bar{y})}{\sqrt{\sum_{i=1}^{N}(x_i-\bar{x})^2}\sqrt{\sum_{i=1}^{N}(y_i-\bar{y})^2}} \quad (4.1)$$

$$\mathrm{RMSE} = \sqrt{\frac{1}{n}\sum_{i=1}^{N}(y_i - x_i)^2} \quad (4.2)$$

where x_i is the pixel value factor, $\bar{x}$ is the average of the pixel value factor, y is water depth, $\bar{y}$ is the average of water depth, N is the number of samples. The Figure 4.4 showed the mean and RMSE of each tree node.

The performance of the regression tree was evaluated as follows: first, the 80 percent of 500 samples joined the training of regression tree model and the remaining 20 percent data were looked as the independent test samples. Second, use the regression tree model to predict another 200 samples as an additional test. They were input to the model for calculating the water depths. The retrieval water depths were compared with the water depth measurements obtained by remote sensing data were shown in Figure. 4.5, and RMSE was 1.085 m. Variables actually used in tree construction were band 2, band1/band2, and ban2-band7. Second, the model was estimated by dividing three ranges in order to evaluate the performance of regression tree model further. Results showed that the regression tree model can effectively predict water depth at less than 5 meters. The MSE were 0.36 to 0.9 meters. However, the accuracy was not ideal for the depth over 5 meters. The MSE of these were 1.09 to 4.39 meters. Compared the observed and predicted water depth of 200 testing data, the RMSE of 0-5 meters, 5-10 meters, more than 10 meters is 1.016 meters, 1.17 meters and 1.22 meters respectively. The relationship of observed and predicted water depth based on regression tree models is shown in Figure 4.6. The R^2 is about 0.85.

```
Node number 6: 43 observations
  mean=10.02283, MSE=4.39215

Node number 8: 38 observations
  mean=1.371699, MSE=0.431711

Node number 9: 18 observations
  mean=3.249032, MSE=0.3598611

Node number 10: 55 observations
  mean=4.694841, MSE=0.9088636

Node number 14: 105 observations
  mean=11.7388, MSE=3.102652

Node number 15: 77 observations
  mean=12.89854, MSE=1.09713

Node number 22: 33 observations
  mean=6.444157, MSE=1.622393

Node number 23: 31 observations
  mean=7.932829, MSE=3.561636
```

Figure 4.4 The Summary of Regression Tree Nodes

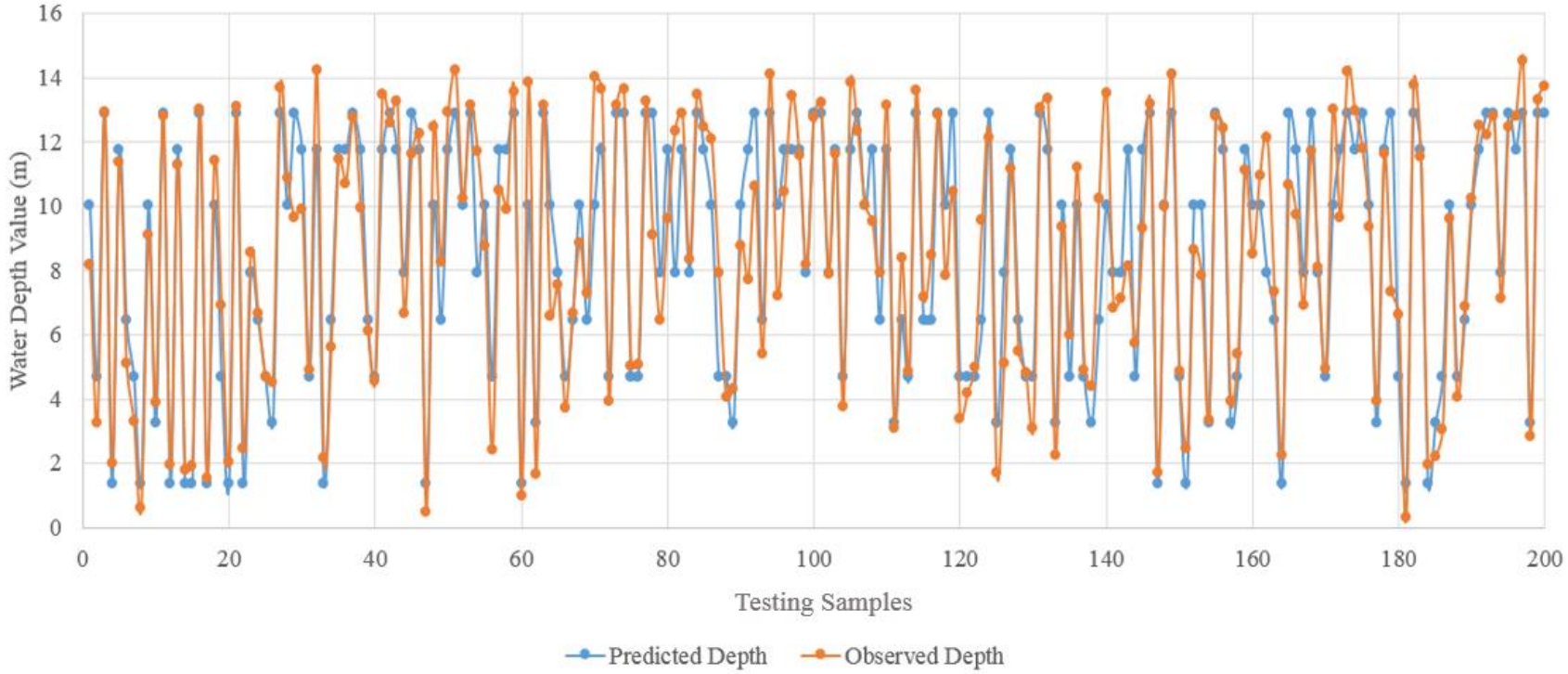

Figure 4.5 Observed and Predicted Water Depth Based on Regression Tree Models

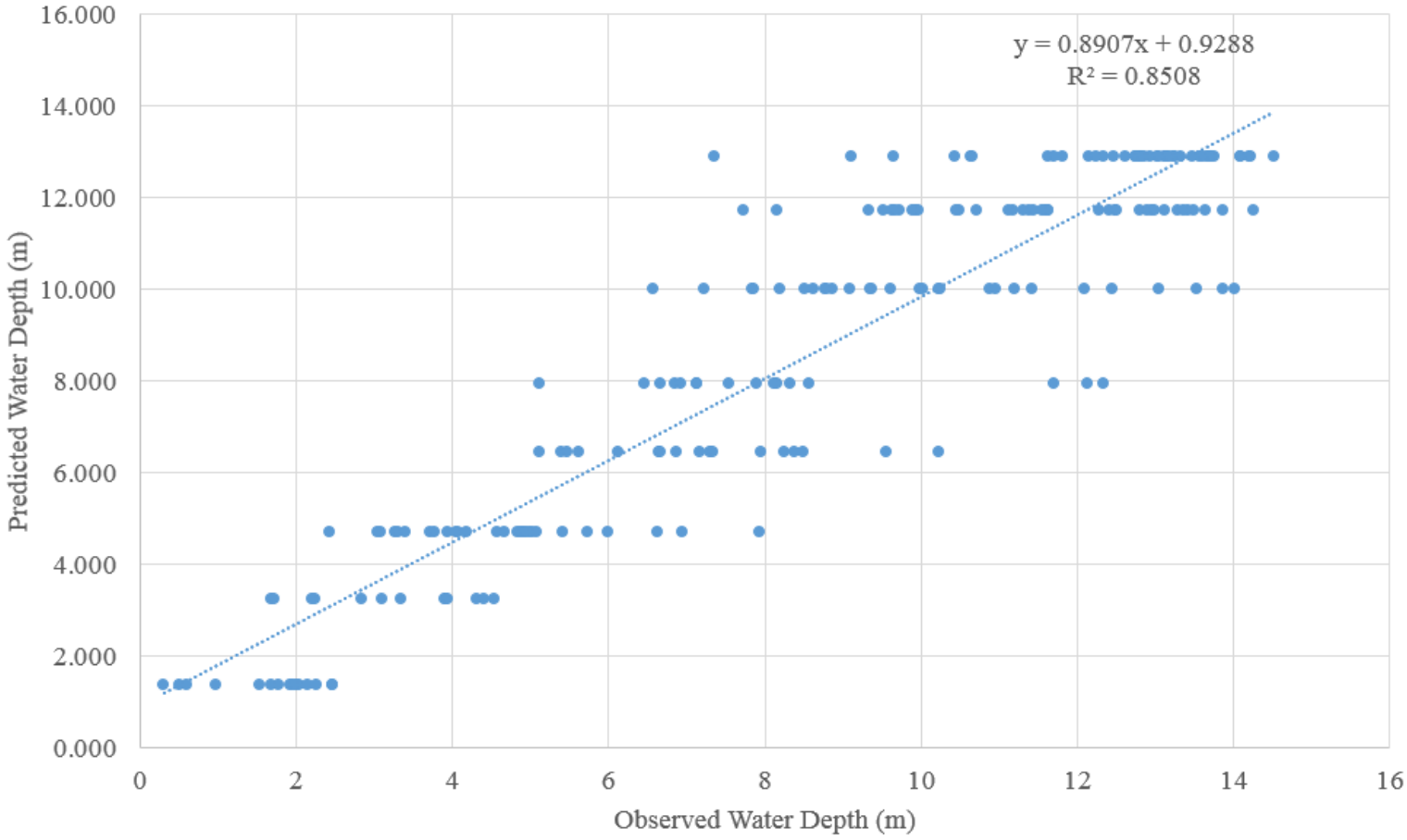

Figure 4.6 The Relationship of Observed and Predicted Water Depth Based on Regression Tree Models

CHAPTER 5. ARTIFICIAL NEURAL NETWORK

Artificial neural networks (ANN), based on the biological neural networks, are information processing methods of simulating behaviors of man brain. Owing to the strong abilities of self-learning, self- organizing, self-adaptability and nonlinear mapping, the ANNs display stronger capabilities of simulating the nonlinear systems than the traditional statistical methods (Long, 1999). The ANN model is an assembly of inter-connected nodes and weighted links. The output node sums up each of its input value according to the weights of its links. Figure 5.1 illustrates a simple neural network architecture known as a perceptome. In this thesis, a back- propagation artificial neural network (BP-ANN) was applied. BP-ANN has a solid theoretical basis and it is widely used in various fields. There are two phases in each iteration of the algorithm: the forward phases and the backward phases.

Forward phases are the computation progresses in the forward direction. During the forward phase, the weights obtained from the previous iteration are used to compute the output value of each neuron in the network. Outputs of the neurons at level k are computed prior to computing the outputs at level k+1. During the backward phase, the weight update formula is applied in the reverse direction. In other words, the weights at level k+1 are updated before the weights at level k are updated. The back-propagation approach allows us to use the errors for neuron at layer k+1 to estimate the error for neurons at layer k (Tan, 2005).

5.1 MODEL BUILDING

In this thesis, a typical three-layered BP-ANN model was developed, including an input layer, a hidden layer and an output layer by MATLAB software. Firstly, the normalization of training data is necessary. “premnmx” function, which is to preprocess data so that the minimum

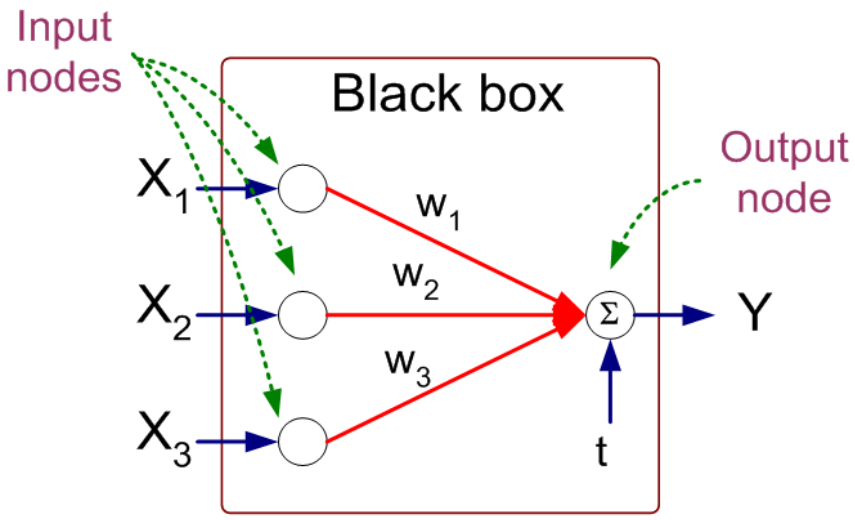

Figure 5.1 The ANN Structure (Tan, 2005)

is -1 and the maximum is 1 was applied. Then, a logarithmic sigmoid transfer function was used for the hidden layer and the linear transfer function was used for the output layer. The training function is "traingdx". "traingdx" is a network training function that updates weight and bias values according to gradient descent momentum and an adaptive learning rate. The single band, band ratios, band differences and band sums selected above used as predictors and the corresponding water depth measurements were predictands. 500 pixel values and water depth measurements were randomly selected as the training samples and 200 pixel values left as test samples. The number of hidden layer neurons and other parameters in the BP-ANN model were determined by continuously learning and training between the predictors and predictands. The relationship between the pixel values and the water depths was established by selecting the optimal weights and biases. Finally, the structure of BP-ANN model was as follows: the number of input, hidden and output layer neurons was 6, 3 and 1 respectively; the learning rate was 0.001; the performance goal was 0.001; the maximum number of epochs to train was 500.

5.2 RESULTS

The performance of the BP-ANN was evaluated the same way as before in the regressiontree models. First, the 80 percent of 500 samples joined the training of BP-ANN model and the remaining 20 percent data were looked as the independent test samples. Second, use the BP-ANN model to predict another 200 samples as an additional test. They were put to the model for calculating the water depths. The retrieval water depths compared with the water depth measurements obtained by remote sensing data were shown in Figure. 5.2. The RMSE was 1.25 m.

Second, the observed water depths were compared with the model retrievals by dividing three ranges in order to evaluate the performance of BP-ANN model further. Results showed that the BPANN model was able to accurately predict water depth if depth is below 5 meters. The RMSE was 0.798 meters. However, the accuracy was not ideal for the depth of 5 to 10 meters. The RMSE was 1.242 meters. The RMSE for the depth of more than 10 meters was 1.01 meters. The relationship of observed and predicted water depth based on ANN models is shown in Figure 5.3. The R^2 is about 0.86.

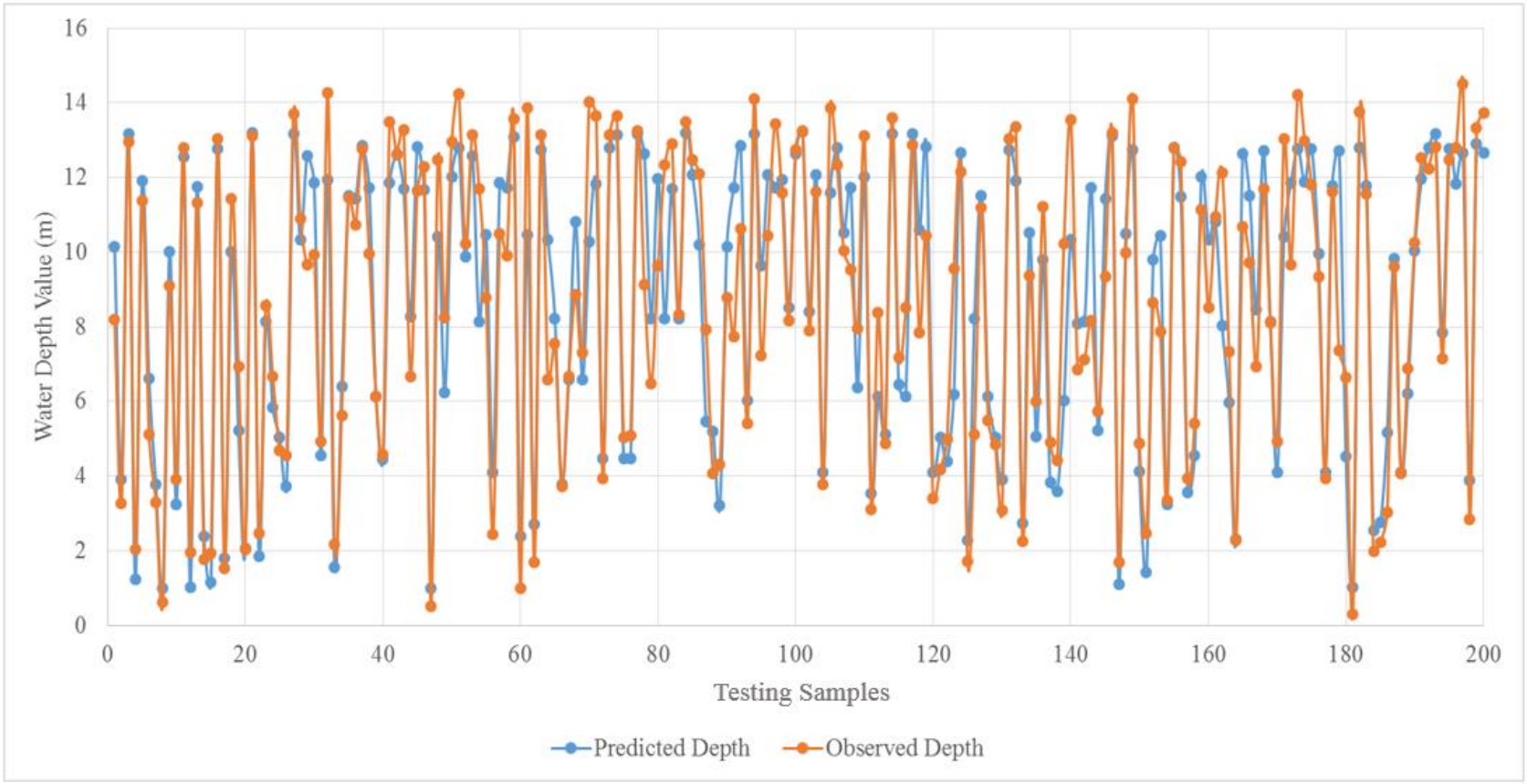

Figure 5.2 Observed and Predicted Water Depth Based on BP-ANN Model

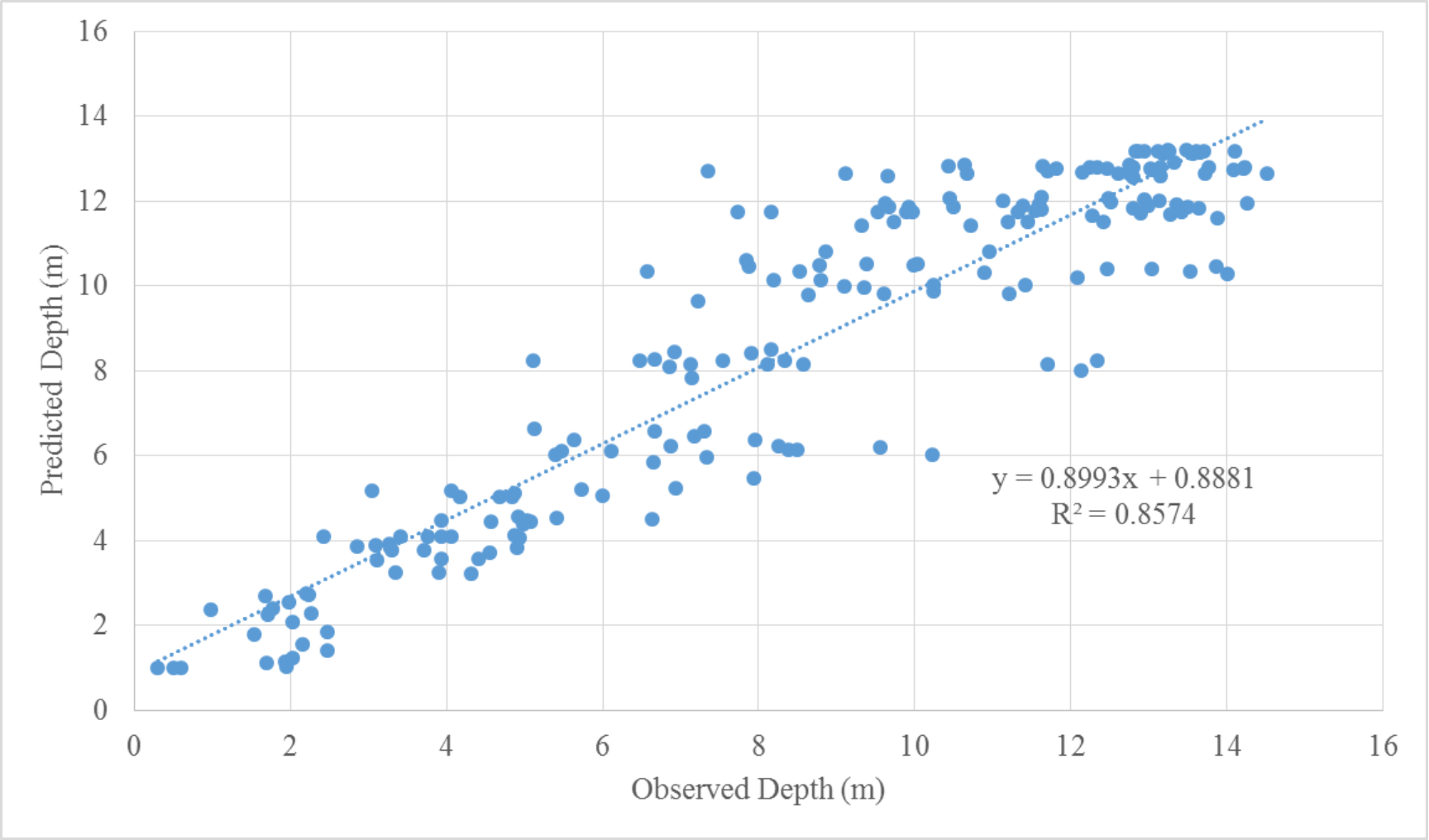

Figure 5.3 The Relationship of Observed and Predicted Water Depth Based on BP-ANN Model

CHAPTER 6. SUPPORT VECTOR REGRESSION

Support Vector Machines is a machine-learning tool, which has been received considerable attention. It has its roots in statistical learning theory. In the literature, there have been many practical uses of SVM (Tan, 2005). Similar to CART, SVM can do both regression and classification. A support vector machine constructs a set of hyperplanes in an infinite dimensional space as classification boundary. The SVM equations are formulated as per Vapnik's theory. The generalization ability of the SVM is considered better than ANN, in the sense that it is based on the structural risk minimization rather than the empirical risk minimization of the ANN (Shiri, 2013). The main process of SVM model building consists of selecting support vectors to support the model structure and determining their weights. The process of an SVM estimator $f(x)$ on regression can be described as:

$$f(x) = \boldsymbol{w}\, \varphi\, (y) + b \qquad (6.1)$$

where **w** is a weight vector, and b a bias, and φ is a nonlinear transfer function mapping the input space into a high-dimensional feature space.

6.1 MODEL BUILDING

In this thesis, I used the Support Vector Machine for regression estimation. Generally, the accuracy of the SVR (Support Vector Regression) model depends on the appropriate selection of kernels and its parameters (Suryanarayana, 2014). In this thesis, four kernel functions were applied for building models. They were “Linear kernel function”, “Gaussian Kernel”, “Polynomial kernel function” and “sigmoid linear kernel function”.

The Linear kernel is the simplest kernel function. It is given by the inner product <x,y>plus an optional constant c. Kernel algorithms using a linear kernel are often equivalent to their non-kernel counterparts.

$$k(\boldsymbol{x}, \boldsymbol{y}) = \boldsymbol{x}^T \boldsymbol{y} + c \qquad (6.2)$$

The Gaussian kernel is an example of radial basis function kernel.

$$k(\boldsymbol{x}, \boldsymbol{y}) = \exp(-\frac{\|\boldsymbol{x}-\boldsymbol{y}\|^2}{2\sigma^2}) \qquad (6.3)$$

The Polynomial kernels are well suited for problems where all the training data is normalized. Adjustable parameters are the slope α, the constant term c and the polynomial degree d.

$$k(\boldsymbol{x}, \boldsymbol{y}) = (\alpha \boldsymbol{x}^T \boldsymbol{y} + c)^d \qquad (6.4)$$

The sigmoid kernel is popular. The formula of sigmoid linear kernel function is as following.

$$k(\boldsymbol{x}, \boldsymbol{y}) = \tanh(\gamma(\boldsymbol{x}^T \boldsymbol{y}) + c) \qquad (6.5)$$

R software was applied for testing these SVM models. It can be generated through the “kernlab” package. There are two commonly used versions of SVM regression, 'eps-SVR' and 'nu-SVR'. Compared the results obtained by the two types, the results showed “eps-SVR” was better than “nu-SVR”. Therefore, the “eps-SVR” was used for the SVM models.

6.2 RESULTS

To evaluate the SVR models, the 10-fold cross-validation sampling strategy was used. 10-fold cross-validation broke data into ten sets of size n/10 and train on nine datasets and test on one.

Then, repeat 10 times and take the mean error rate. All the four kernel types were tested on the validation data. The results are listed in Table 6.1. The retrieval water depths by four SVM models compared with the water depth measurements obtained by remote sensing data are shown in Figure. 6.1, Figure 6.3, Figure 6.5 and Figure 6.7. The RMSE of "Linear kernel function" was 1.27 m; the RMSE of "Gaussian Kernel" was 1.08 m; the RMSE of "Polynomial kernel function" was 1.13 m; and the RMSE of "sigmoid linear kernel function" was 1.04 m. The RMSEs in different water depth ranges are shown in Table. The relationships of observed and predicted water depth based on four kinds SVM models are shown in Figure 6.2, Figure 6.4, Figure 6.6 and Figure 6.8. The R^2 are about 0.81, 0.86, 0.83 and 0.83 respectively.

Table 6.1 The RMSE of SVM Models Using Different Kernel Functions

Kernel Function	RMSE (0-5 meters)	RMSE (5-10 meters)	RMSE (>10 meters)
Linear	1.31	1.22	1.16
Gaussian	0.80	1.22	1.09
Polynomial	0.93	1.10	1.23
Sigmoid	0.87	1.256	1.14

Figure 6.1 Observed and Predicted Water Depth Based on SVM (Linear Kernel)

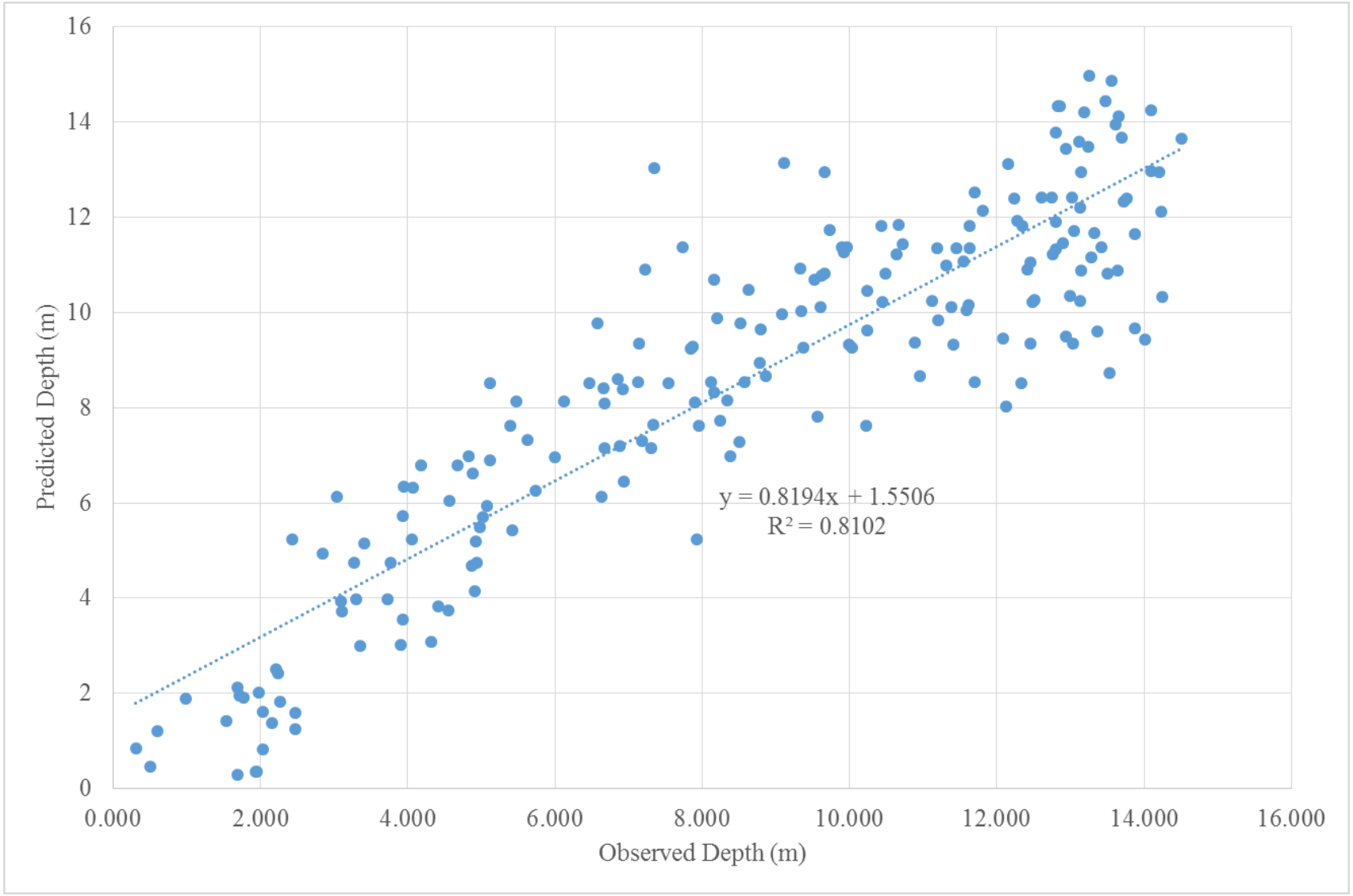

Figure 6.2 The Relationship of Observed and Predicted Water Depth Based on SVM (Linear Kernel)

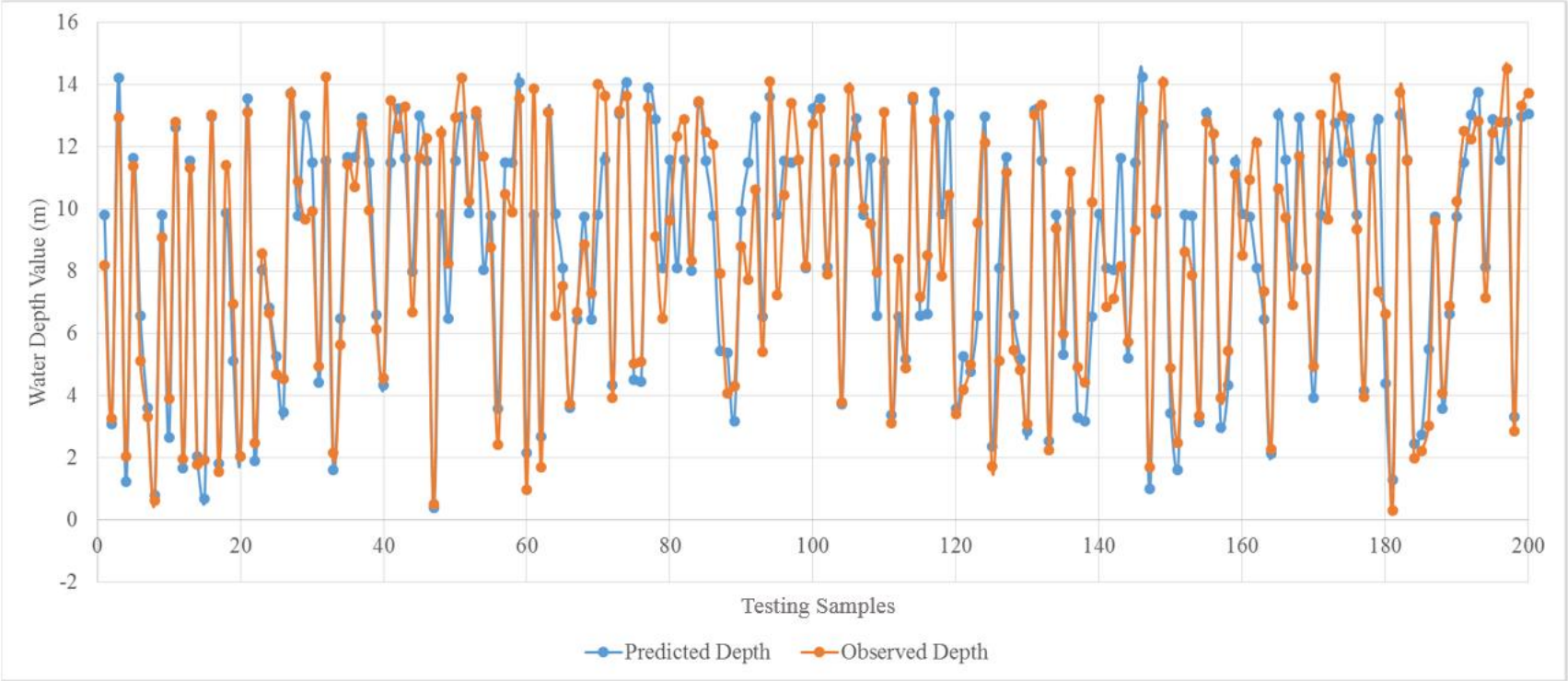

Figure 6.3 Observed and Predicted Water Depth Based on SVM (Gaussian kernel)

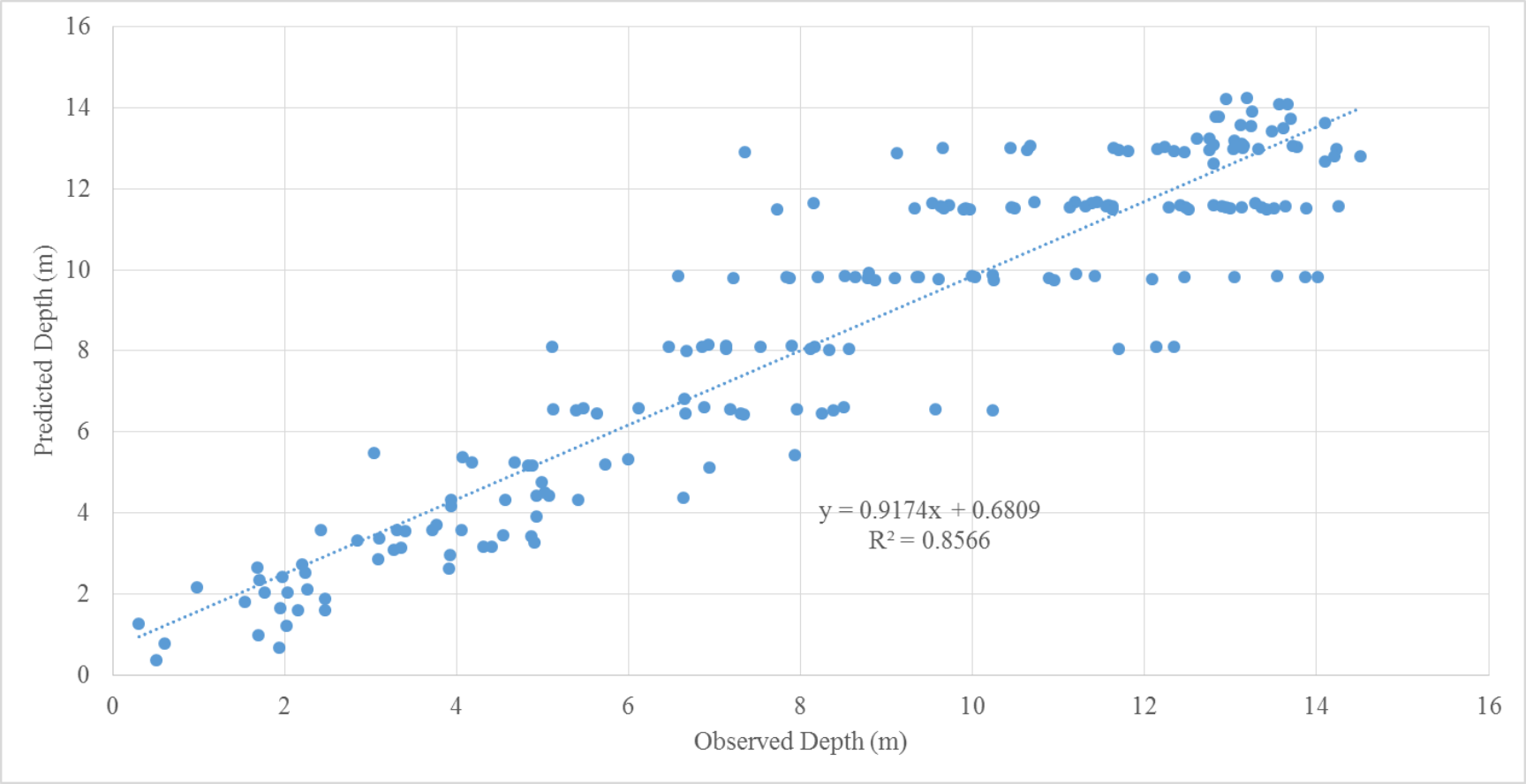

Figure 6.4 The Relationship of Observed and Predicted Water Depth Based on SVM (Gaussian kernel)

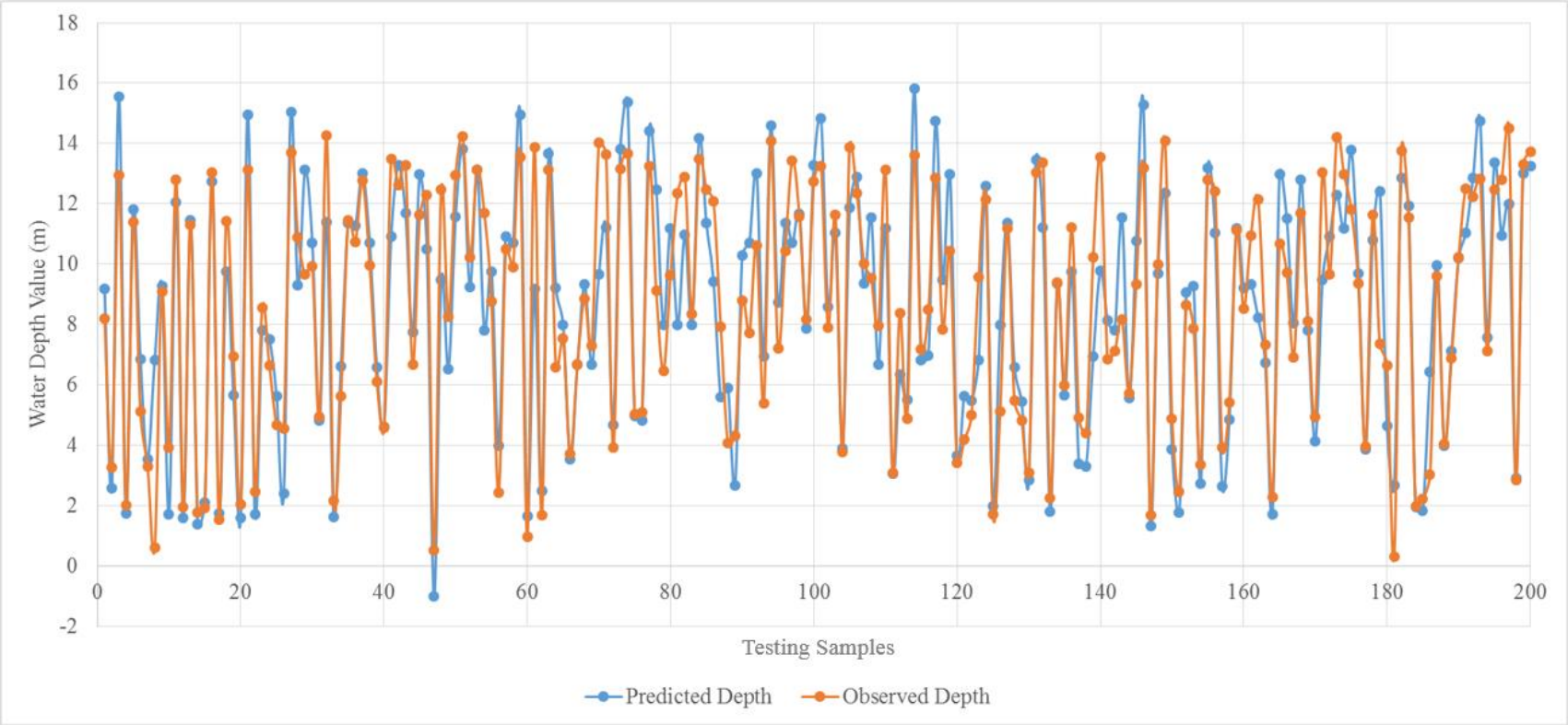

Figure 6.5 Observed and Predicted Water Depth Based on SVM (Polynomial Kernel)

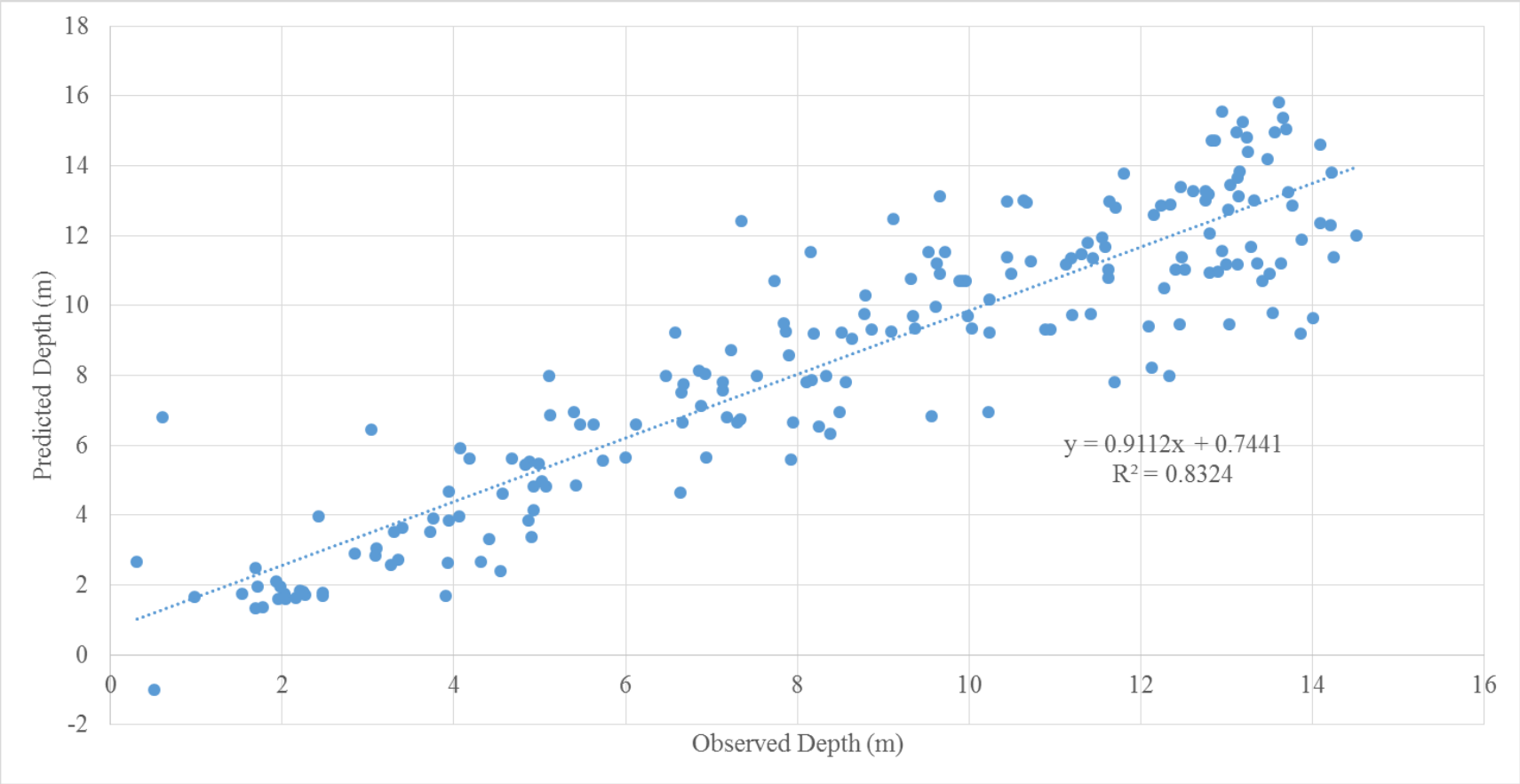

Figure 6.6 The Relationship of Observed and Predicted Water Depth Based on SVM (Polynomial Kernel)

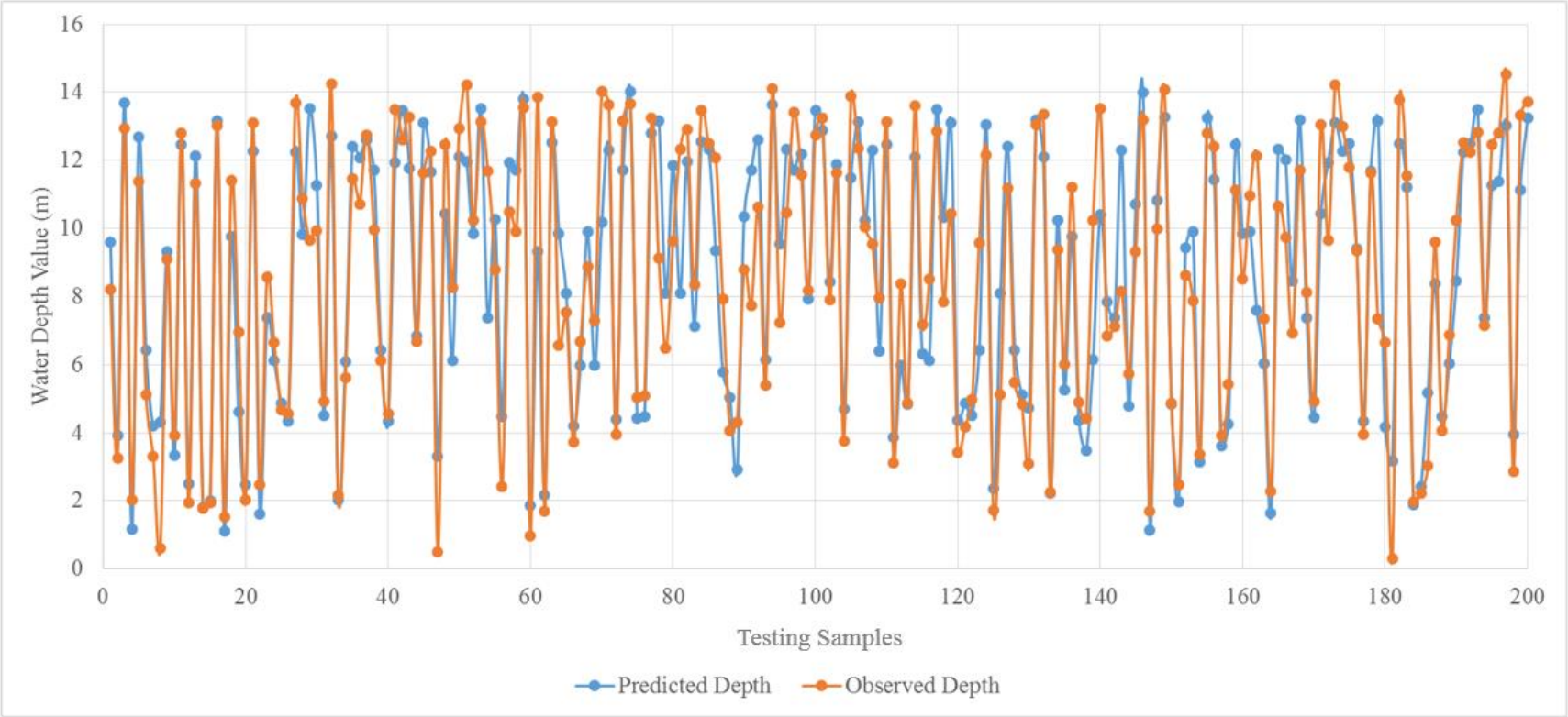

Figure 6.7 Observed and Predicted Water Depth Based on SVM (Sigmoid)

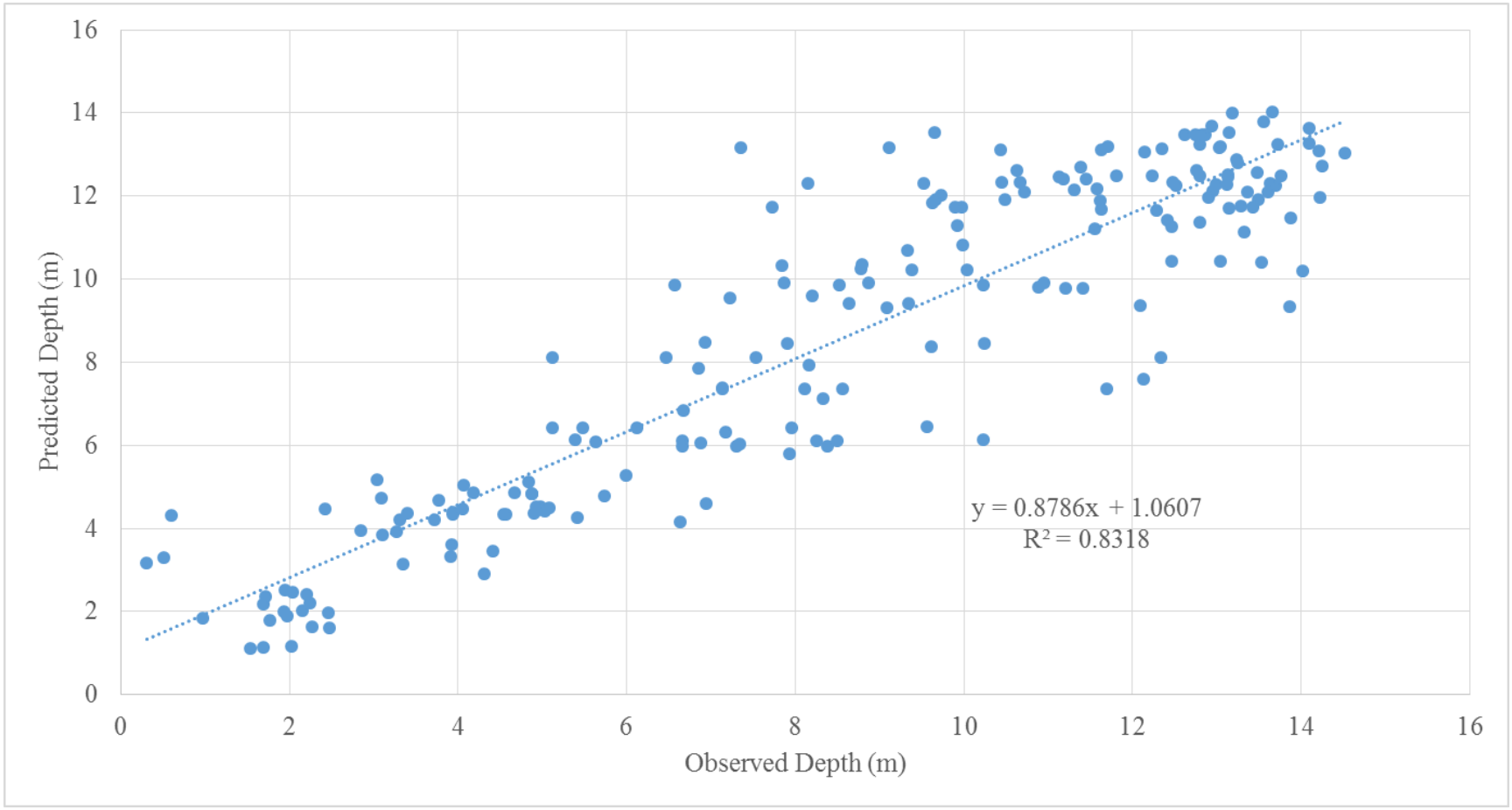

Figure 6.8 The Relationship of Observed and Predicted Water Depth Based on SVM (Sigmoid)

CHAPTER 7. CONCLUSION

A regression tree model, a BP-ANN model and several SVMs models with different kernel functions were developed for water depth inversion from Landsat remote sensing image. The results can be summarized as below:

(1) Machine learning algorithms are better than regression models in general when dealing with non-linear problems. This research tested all the mostly used machine-learning methods for water depth retrieval. All three algorithms were capable of retrieving water depth data at reasonable accuracy.

(2) The data mining models established using the relationship between pixel value derived from satellite data and water depths obtained from ICESat and Bathymetric LiDAR data in a southeastern part of Lake Michigan. The uses of laser altimetry data ensures high accuracy of elevation measures.

(3) Overall, for all models, the R^2s of them are greater than 0.85. The RMSE of the regression tree model and the SVM model with a Gaussian kernel were smaller than other models.

(4) All the models had better accuracy at water depth < 5 m than deeper depth areas. However, the accuracy was not unsatisfactory for the depth from 5 to 10 meters. The RMSE for the depth of more than 10 meters is better than that the depth of 5 to 10 meters.

(5) Compare among all the machine-learning models, the SVM model with Gaussian kernel function had the best accuracy.

REFERENCE

Bellian, J., Kerans, C., & Jennette, D. (2005). Digital Outcrop Models: Applications of Terrestrial Scanning Lidar Technology in Stratigraphic Modeling. *Journal of Sedimentary Research, 75*(2), 166-176.

Bierwirth, P.N., T.J. Lee and R.V. Burne. (1993). Shallow Sea-Floor Reflectance and Water DepthDerived by Unmixing Multispectral Imagery. *Photogrammetric Engineering &RemoteSensing, 59*(3), 331-338.

Breiman, L. (1984). *Classification and regression trees*. Belmont, Calif.: Wadsworth International Group.

Buckley, S., Howell, J., Enge, H., & Kurz, T. (2008). Terrestrial laser scanning in geology: Data acquisition, processing and accuracy considerations. *Journal of the Geological Society, 165*, 625-638.

Campbell, J. (2007). *Introduction to remote sensing* (5th ed.). New York: Guilford Press.

Chang, C., Liu, C., Chung, H., Lee, L., & Yang, W. (n.d.). Development and evaluation of a genetic algorithm-based ocean color inversion model for simultaneously retrieving optical properties and bottom types in coral reef regions. *Appl. Opt. Applied Optics, 53*(4), 605-617.

Chipman, J., & Lillesand, T. (2007). Satellite-based assessment of the dynamics of new lakes in southern Egypt. *International Journal of Remote Sensing*, 4365-4379.

Conger, C., Hochberg, E., Fletcher, C., & Atkinson, M. (2006.). Decorrelating remote sensing color bands from bathymetry in optically shallow waters. *IEEE Trans. Geosci. Remote Sensing IEEE Transactions on Geoscience and Remote Sensing, 44*, 1655-1660.

Dong, L., Li, G., & Tang, S. (2011). Inversion of forest canopy height in south of China by integrating GLAS and MERSI: The case of Jiangxi province in China. *Journal of Remote Sensing, 15*(6), 1301-1314.

Doxani, G., Papadopoulou, M., Lafazani, P., Pikridas, C., & Tsakiri-Strati, M. (2012). Shallow-Water Bathymetry Over Variable Bottom Types Using Multispectral Worldview-2 Image. *International Archives of the Photogrammetry, Remote Sensing and Spatial Information Sciences,* 159-164.

Fan, K., Huang, W., He, M., Fu, B., Zhang, B., & Chen, X. (2008). Depth inversion in coastal water based on SAR image of waves. *Chin. J. Ocean. Limnol. Chinese Journal of Oceanology and Limnology, 26*(4), 434-439.

Hodgetts, D. (2009). LiDAR in the Environmental Sciences: Geological Applications. *Laser Scanning for the Environmental Sciences,* 165-179.

Höfle, B., & Rutzinger, M. (2011). Topographic airborne LiDAR in geomorphology: A technological perspective. *Zeit Fur Geo Supp Zeitschrift Für Geomorphologie, Supplementary Issues, 55*(2), 1-29.

Introduction to Remote Sensing. Retrieved from http://lms.seos-project.eu/learning_modules/remotesensing/remotesensing-c01-p05.html.

Legleiter, C. (2011). Remote measurement of river morphology via fusion of LiDAR topography and spectrally based bathymetry. *Earth Surf. Process. Landforms Earth Surface Processes and Landforms, 37*(5), 499-518.

Liu, S., Gao, Y., Zheng, W., & Li, X. (2015). Performance of two neural network models in bathymetry. *Remote Sensing Letters, 6*(4), 321-330.

Liu, S., Zhang, J., & Ma, Y. (2010). Bathymetric ability of SPOT-5 multi-spectral image in shallow coastal water. *2010 18th International Conference on Geoinformatics,* 1-5.

Long, J., Ning, C. & Lin, Z. (1999). Study and comparison of ensemble forecasting based on artificial neural network. *Acta meteorologica sinica,*198-207.

Lyzenga, D. (1978). Passive remote sensing techniques for mapping water depth and bottom features. *Appl. Opt. Applied Optics, 17*(3), 379-383.

Lyzenga, D. (1981). Remote sensing of bottom reflectance and water attenuation parameters in shallow water using aircraft and Landsat data. *International Journal of Remote Sensing, 2*(1), 71-82.

Lyzenga, D. (1985). Shallow-water bathymetry using combined lidar and passive multispectral scanner data. *International Journal of Remote Sensing, 6*(1), 115-125.

Poupardin, A., Michele, M., Raucoules, D., & Idier, D. (2014). Water depth inversion from satellite dataset. *2014 IEEE Geoscience and Remote Sensing Symposium,* 2277-2280.

Raj, A. & Sabu, P. (2013). Shallow Water Bathymetry using Log-linear Inversion Technique: A Case Study at Vizhinjam. *International Journal of Innovative Research in Science, Engineering and Technology, 2*(1), 223-230.

Reif, M., Wozencraft, J., Dunkin, L., Sylvester, C., & Macon, C. (2013). A review of U.S. Army Corps of Engineers airborne coastal mapping in the Great Lakes. *Journal of Great Lakes Research, 39,* 194-204.

Sandidge, J., & Holyer, R. (1998). Coastal Bathymetry from Hyperspectral Observations of Water Radiance. *Remote Sensing of Environment, 65*(3), 341-352.

Schutz, B., Zwally, H., Shuman, C., Hancock, D., & Dimarzio, J. (2005). Overview of the ICESat Mission. *Geophysical Research Letters, 32*(21), 1-4.

Shiri, J., Kisi, O., Yoon, H., Lee, K., & Nazemi, A. (2013). Predicting groundwater level fluctuations with meteorological effect implications—A comparative study among soft computing techniques. *Computers & Geosciences, 56*, 32-44.

Smola, A., Schölkopf, B., & Müller, K. (1998). Convex Cost Functions for Support Vector Regression. *ICANN 98 Perspectives in Neural Computing*, 99-104.

Srivastava, P. (2014). *Remote sensing applications in environmental research*. Springer.

Stumpf, R., Holderied, K., & Sinclair, M. (2003). Determination of water depth with high-resolution satellite imagery over variable bottom types. *Limnol. Oceanogr. Limnology and Oceanography, 48*(1), 547-556.

Su, H., Liu, H., & Heyman, W. (2008). Automated Derivation of Bathymetric Information from Multi-Spectral Satellite Imagery Using a Non-Linear Inversion Model. *Marine Geodesy, 31*, 281-298.

Suryanarayana, C., Sudheer, C., Mahammood, V., & Panigrahi, B. (2014). An integrated wavelet-support vector machine for groundwater level prediction in Visakhapatnam, India. *Neurocomputing, 145*, 324-335.

Tan, P., & Steinbach, M. (2005). *Introduction to data mining*. Boston: Pearson Addison Wesley.

Thomas, S., Mcgwire, K., Lutz, A., Kratt, C., Trammell, E., Thomas, J., & Mckay, W. (2012). Geospatial and regression tree analysis to map groundwater depth for manual well drilling suitability in the Zinder region of Niger. *Journal of Hydrology, 446-447*, 35-47.

Vojinovic, Z., Abebe, Y., Ranasinghe, R., Vacher, A., Martens, P., Mandl, D., Frye, S., Ettinger, E. & Zeeuw, R. (2013). A machine learning approach for estimation of shallow water depths from optical satellite images and sonar measurements. *Journal of Hydroinformatics, 15*, 1408-1424.

Wang, X., Cheng, X., Gong, P., Huang, H., Li, Z., & Li, X. (2011). Earth science applications of ICESat/GLAS: A review. *International Journal of Remote Sensing, 32*(23), 8837-8864.

Wang, Y., Zhang, P., Dong, W. & Zhang Y. (2007). Study on Remote Sensing of Water Depths Based on BP Artificial Neural Network. *Marine Science Bulletin*, *9*, 26-34.

Weeks, S., Werdell, P., Schaffelke, B., Canto, M., Lee, Z., Wilding, J., & Feldman, G. (2012). Satellite-Derived Photic Depth on the Great Barrier Reef: Spatio-Temporal Patterns of Water Clarity. *Remote Sensing, 4*(12), 3781-3795.

Yasa, R., & Etemad-Shahidi, A. (2013). Classification and Regression Trees Approach for Predicting Current-Induced Scour Depth Under Pipelines. *J. Offshore Mech. Arct. Eng. Journal of Offshore Mechanics and Arctic Engineering, 136*(1), 1-8.

Zhang, M., Zhu, S., Zeng, W., & Zhang, W. (2013). Water Depth Inversion in Sanya Bay Based on TM Image. *AMM Applied Mechanics and Materials, 392*, 962-965.

Zhang, Z., & Teng, H. (2011). An Inversion Method of Remote Sensing Water Depth Based on Transmission Bands Ratio. *2011 Fourth International Joint Conference on Computational Sciences and Optimization*, 1002-1006.

Zwally, H., Schutz, B., Abdalati, W., Abshire, J., Bentley, C., Brenner, A., . . . Thomas, R. (2002). ICESat's laser measurements of polar ice, atmosphere, ocean, and land. *Journal of Geodynamics, 34*(3-4), 405-445.

VITA

Shu Gao is from Qingdao, People's Republic of China. She earned her bachelor degree in Geomatics Engineering from China University of Petroleum (East China), 2013. During that time, she was greatly influenced by outstanding faculty members Dr. Jianhua Wan and Dr. Shanwei Liu both played large roles in Shu's decision to pursue an advanced degree.

After graduation of undergraduate, Shu entered the graduate program at Louisiana State University with Dr. Lei Wang as his primary advisor. In August 2015, Shu began to pursue her Ph.D. degree in Coastal Engineering at LSU with Dr. Hagen.

Shu plans to graduate LSU with the degree of Masters of Science in Geography in the fall of 2015.